Statistical Delay and Error-Rate Bounded QoS Provisioning for SWIPT Over CF M-MIMO 6G Mobile Wireless Networks Using FBC

Xi Zhang, *Fellow, IEEE*, Jingqing Wang, and H. Vincent Poor, *Life Fellow, IEEE*

***Abstract*—As a new and dominating type of time-sensitive traffic over 6G wireless networks, massive ultra-reliable and low latency communications (mURLLC) has attracted considerable research attention, while raising several new challenges, including massive connectivity, ultra-low latency, super-reliability, and high energy efficiency. Several promising 6G enablers, including statistical delay and error-rate bounded quality-of-service (QoS) provisioning, cell-free (CF) massive multi-input multi-output (m-MIMO), simultaneous wireless information and power transfer (SWIPT), etc., have been developed to support mURLLC. Specifically, CF m-MIMO can significantly enhance QoS performance of SWIPT by boosting data rate and energy efficiency. On the other hand, finite blocklength coding (FBC) has been proposed to support various massive access techniques while reducing access latency and guaranteeing stringent QoS. However, how to efficiently integrate SWIPT with CF m-MIMO using FBC for statistical delay and error-rate bounded QoS to support mURLLC has posed many new challenges not encountered before. To overcome these difficulties, in this paper we develop FBC based statistical delay and error-rate bounded QoS provisioning schemes over SWIPT-enabled CF m-MIMO 6G wireless networks. First, we establish SWIPT-enabled CF m-MIMO system models using FBC. Then, we optimize the tradeoffs between ϵ-effective capacity and harvested energy for our proposed statistical QoS provisioning. Finally, simulation results validate and evaluate our developed schemes.**

***Index Terms*—Statistical delay and error-rate bounded QoS, SWIPT, CF m-MIMO, FBC, ϵ-effective capacity vs. energy, 6G.**

I. Introduction

With the growing demands for delay-sensitive 6G wireless multimedia services, it is critical to develop wireless network architectures in supporting new 6G massive ultra-reliable and low-latency communications (mURLLC) [1], [2] traffic while guaranteeing various quality-of-service (QoS) requirements. However, with the exponentially increasing demand for bandwidth-intensive and delay-sensitive multimedia traffic under stringent QoS requirements, the implementation of 6G wireless networks has imposed many new challenges and research opportunities as well, including massive connectivity, bounded end-to-end delay, super-reliability, constrained power/battery supply, and radio frequency (RF) wireless power transfer [3].

Towards this end, inspired by the theories of large deviations and effective bandwidths, the statistical delay-bounded QoS theory [4]–[14] has been proposed as a promising technique to model and control the queueing behaviors of wireless fading channels, and characterize stochastic performance bounds on wireless traffic in supporting the time-sensitive wireless multimedia applications. In addition, the major design issue raised by mURLLC is how to support latency-sensitive multimedia transmissions, while guaranteeing a reliability bound over time-varying wireless channels. Along this direction, considering finite blocklength data transmissions with non-vanishing error probability, finite blocklength coding (FBC) [15] has been proposed to support various massive access techniques while reducing the access latency and guaranteeing stringent QoS requirements. The existing works have shown that the codeword blocklength can be as short as 100 channel symbols for reliable data transmission [16]. The authors of [17] have derived the goodput over additive white Gaussian noise (AWGN) channels as well as the energy-efficiency spectral-efficiency tradeoff using recent results of FBC. The authors of [18] have characterized the maximum achievable data rate over quasi-static multi-input multi-output (MIMO) based wireless fading channels in the finite blocklength regime. The authors of [19] have derived closed-form expressions for error probability/throughput and determined the minimum number of antennas to satisfy different error probability/throughput requirements for MIMO systems using FBC.

On the other hand, one of the challenges that can potentially limit the widespread deployment of mURLLC-enabled 6G wireless networks is the constrained power/battery supply of the mobile devices. To solve this problem, taking advantage of the broadcast nature of RF wave propagation, simultaneous wireless information and power transfer (SWIPT) [20]–[22], which

Manuscript received January 17, 2021; revised May 26, 2021; accepted June 5, 2021. Date of publication July 19, 2021; date of current version October 4, 2021. The work of Xi Zhang and Jingqing Wang was supported in part by U.S. National Science Foundation under Grants: CCF-2142890, CCF-2008975, ECCS-1408601 and CNS-1205726, and in part by U.S. Air Force under Grant FA9453-15-C-0423. The work of H. Vincent Poor was supported by U.S. National Science Foundation under Grants: CCF-0939370 and CCF-1908308. The guest editor coordinating the review of this manuscript and approving it for publication was Prof. Sennur Ulukus. *(Corresponding author: Xi Zhang.)*

Xi Zhang and Jingqing Wang are with the Networking and Information Systems Laboratory, Department of Electrical and Computer Engineering, Texas A&M University, College Station, TX 77843 USA (e-mail: xizhang@ece.tamu.edu; wang12078@tamu.edu).

H. Vincent Poor is with the Department of Electrical and Computer Engineering, Princeton University, Princeton, NJ 08544 USA (e-mail: poor@princeton.edu).

Digital Object Identifier 10.1109/JSTSP.2021.3097898

transfers both information and power simultaneously to mobile devices, has recently gained significant research attention since it can prolong the battery-life of energy-constrained and low-power-supported mobile devices. Unlike recievers that separate information and energy transmissions researchers have developed two main low-complexity co-located receiver structures, i.e., the power-splitting (PS) receiver and the time-switching (TS) receiver for enabling SWIPT. In the PS receiver, the power and information transfer to the co-located energy harvesting (EH) and information decoding receivers are simultaneously achieved via a set of power splitting devices. On the other hand, each transmission block is split into two orthogonal time-slots for information and energy transmissions in the TS receiver.

There have been a number of works focusing on investigating the SWIPT technique to support mURLLC. In particular, the authors of [23] have conducted a comprehensive survey of the state-of-art techniques based on advances and open issues imposed by SWIPT. The authors of [24] have analyzed the fundamental tradeoff between transmitting energy and information over a single noisy line. In addition, ultra reliable cooperative short packet communication schemes have been investigated in [25] with wireless power transfer (WPT) to support mURLLC. The authors of [26] have analyzed the performance of a non-orthogonal SWIPT-enabled system using FBC and derived novel analytical expressions for the end-to-end average block error probability. The authors of [27] have analyzed a WPT system with finite blocklength and finite power/battery supply under Nakagami-m wireless fading channels. The authors of [28] have characterized the fundamental limits of SWIPT in terms of the information-energy capacity region in the non-asymptotic regime. The authors of [29] have investigated the rate-energy tradeoff and the decoding error probability-energy tradeoff for SWIPT systems in the finite blocklength realm.

However, one of the major bottlenecks for implementing SWIPT is the low harvested energy levels due to the inherent severe end-to-end path-loss at the receiver. Towards this end, the application of conventional co-located massive MIMO (m-MIMO) techniques can enhance the performance of SWIPT in terms of the achievable data rate and energy efficiency due to its benefits of favorable propagation, channel hardening, and aggressive spatial multiplexing gains. In addition, in distributed m-MIMO systems, service antennas are spread out over a large area, which provide with significantly higher probability of coverage than the conventional collocated m-MIMO systems, at the cost of increased backhaul network overhead. However, inter-cell interference is becoming the major bottleneck for m-MIMO systems, especially for dense mobile wireless networks. To resolve the interference issues in current cellular networks, as one of the promising 6G network architectures, *cell-free massive MIMO* (CF m-MIMO) [30]–[32], where geographically distributed access points (APs) coherently serve all users using the same time-frequency resources, has been proposed to support mURLLC. One of the important features of CF m-MIMO lies in its operating regime: a very large number of single-antenna APs simultaneously and *cooperatively* (through a central processing unit (CPU)) serve a relatively smaller number of mobile users, performing computationally simple signal processing at the APs. Specifically, compared with traditional co-located m-MIMO systems, CF m-MIMO can leverage the benefits of macro-diversity to mitigate shadow fading more efficiently since the APs are distributed over a large geographical area. Due to the closer distance between the APs and mobile devices, integrating SWIPT with CF m-MIMO systems has a significant potential to offer substantially higher coverage probability while minimizing the throughput/energy outage probabilities as compared with co-located m-MIMO systems.

Since CF m-MIMO has been shown to be much more robust to correlated small/large-scale fading as compared with the co-located m-MIMO systems [31], the CF m-MIMO can significantly boost the performance gains of SWIPT. Although there has been substantial research on integrating SWIPT with co-located massive MIMO, only a limited number of studies have focused on investigating SWIPT-driven CF m-MIMO based system models. In particular, the performance of SWIPT-driven CF m-MIMO schemes has been characterized in [33]. The authors of [34] have shown that the achievable energy-rate trade-off of SWIPT can be significantly enhanced by employing the CF m-MIMO technique. A secure SWIPT-enabled CF m-MIMO system is presented in [35]. However, how to efficiently integrate SWIPT with CF m-MIMO architecture models while supporting mURLLC traffic in the finite blocklength regime is still an open problem over 6G wireless networks.

To effectively overcome the above-mentioned challenges, in this paper we propose and develop statistical delay and error-rate bounded QoS provisioning schemes over SWIPT-enabled CF m-MIMO 6G wireless networks in the finite blocklength regime. In particular, we establish SWIPT-enabled CF m-MIMO based system models through employing FBC. We also quantitatively characterize the fundamental tradeoff between harvested energy and ϵ-effective capacity for statistical delay and error-rate bounded QoS provisioning. Furthermore, we formulate and solve optimization problems for the tradeoff between the ϵ-effective capacity and harvested energy under both TS and PS protocols by developing joint optimization algorithms in supporting 6G mURLLC. Also conducted is a set of simulations to validate and evaluate our proposed schemes over SWIPT-enabled CF m-MIMO based 6G wireless networks.

Our main contributions in this paper are summarized as follows:

- We develop statistical delay and error-rate bounded QoS provisioning schemes over SWIPT-enabled CF m-MIMO 6G wireless networks in the finite blocklength regime.
- We establish SWIPT-enabled CF m-MIMO based system models for uplink pilot training, downlink SWIPT, and downlink data transmissions using FBC.
- We define the ϵ-effective capacity-energy region under both TS and PS protocols and quantitatively characterize the fundamental tradeoff between harvested energy and ϵ-effective capacity for statistical delay and error-rate bounded QoS provisioning.
- We formulate and solve the optimal ϵ-effective capacity-energy tradeoff problems for SWIPT-enabled schemes

TABLE I
SUMMARY OF ABBREVIATIONS

mURLLC	massive ultra-reliable and low-latency communications
QoS	quality-of-service
CF	cell-free
m-MIMO	massive multi-input multi-output
SWIPT	simultaneous wireless information and power transfer
FBC	finite blocklength coding
RF	radio frequency
PS	power-splitting
TS	time-switching
EH	energy harvesting
WPT	wireless power transfer
APs	access points
CPU	central processing unit
MMSE	minimum mean-squared error
SNR	signal-to-noise radio
LDP	large deviation principle
R-E	rate-energy
SCA	successive convex approximation

with power allocation for statistical delay and error-rate bounded QoS provisioning under both TS and PS protocols by developing joint optimization algorithms for 6G mURLLC in finite blocklength regime.

The rest of this paper is organized as follows: Section II establishes SWIPT-enabled CF m-MIMO based system models. Section III formulates and solves the optimization problems for the tradeoff between downlink ϵ-effective capacity and harvested energy. Section IV formulates and solves the joint optimization problems for the tradeoff between uplink ϵ-effective capacity and harvested energy. Section V evaluates and analyzes the system performance for our proposed SWIPT-enabled CF m-MIMO schemes. The paper concludes with Section VI.

The summary of abbreviations is listed in Table I. The summary of notation is listed in Table II in Appendix A.

II. The System Models

Fig. 1 shows the system architecture model for our proposed SWIPT-enabled CF m-MIMO 6G wireless networks, where each mobile device is served by coherent joint transmissions from all APs. Assume that there are K_{a} randomly located APs over a large area and K_{u} mobile devices. Assume that the APs are equipped with N_{T} antennas while each mobile user is equipped with a single antenna. All APs are connected to a CPU through backhaul links. We adopt the TS and PS receivers at the mobile devices. We assume that the system operates in a time-slotted fashion, where time is divided into frames. Each frame is divided into three main orthogonal phases, i.e., uplink pilot training, downlink SWIPT transmission, and uplink data transmission, as follows.

1) *Uplink pilot training phase:* Define n_{p} as the number of channel uses for uplink pilot training phase. The mobile devices send pilot signals to the APs for channel estimation during the uplink pilot training phase over n_{p} channel uses;
2) *Downlink SWIPT phase:* By adopting the TS and PS receivers, the downlink SWIPT phase is divided into two sub-phases based on the TS factor, denoted by α, and PS factor, denoted by ρ. Define n_{d} as the number of channel uses for downlink SWIPT phase. As shown in Fig. 1, in the first downlink power transfer sub-phase, the mobile devices harvest energy from the APs over αn_{d} channel uses by using TS protocol. Each mobile device performs as a pure EH receiver and harvests energy from the APs. In the second downlink information transfer sub-phase, the remaining $(1-\alpha)n_{\mathrm{d}}$ channel uses are allocated for simultaneous downlink information transfer by using PS protocol with the PS factor ρ.
3) *Uplink data transmission phase:* Define n_{u} as the number of channel uses for the uplink data transmission from the mobile devices to the APs. During the uplink data transmission phase, each mobile device transmits the finite-blocklength data to the APs using the energy harvested in the previous downlink SWIPT phase.

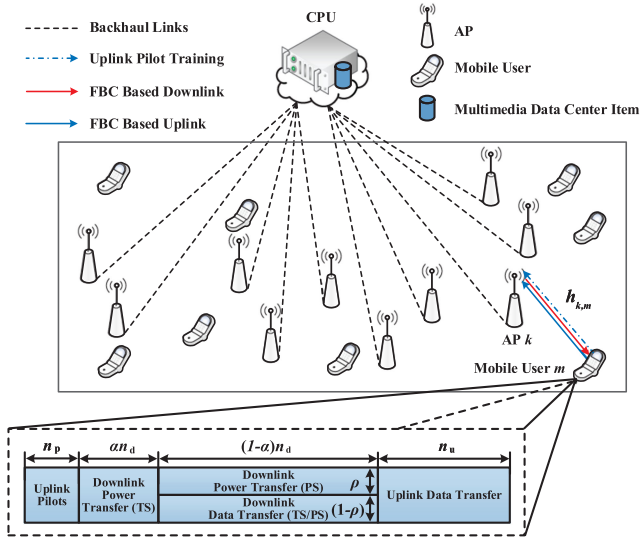

Fig. 1. The system architecture model for our proposed SWIPT-enabled CF m-MIMO based 6G wireless networks in the finite blocklength regime, where n_{p}, n_{d}, and n_{u} are the number of channel uses for uplink pilot training phase, downlink SWIPT phase, and uplink data transmission phase, respectively, and α and ρ are the TS and PS factors, respectively.

A. Uplink Pilot Training

We can derive the channel's impulse response vector, denoted by $\boldsymbol{h}_{k,m} \in \mathbb{C}^{N_{\mathrm{T}}\times 1}$, from mobile device m $(m = 1, \ldots, K_{\mathrm{u}})$ to AP k $(k = 1, \ldots, K_{\mathrm{a}})$ as follows:

$$\boldsymbol{h}_{k,m} = \sqrt{\beta_{k,m}}\boldsymbol{g}_{k,m} \tag{1}$$

where $\beta_{k,m}$ denotes the large-scale fading coefficient from mobile device m to AP k and $\boldsymbol{g}_{k,m} \sim \mathcal{C}N(\mathbf{0}, \mathbf{I}_{N_{\mathrm{T}}})$ represents the small-scale Rayleigh fading vector from mobile device m to AP k, where $\mathbf{I}_{N_{\mathrm{T}}}$ is the identity matrix of size N_{T}. Define the pilot training sequence transmitted from mobile device m as $\boldsymbol{\phi}_m^{n_{\mathrm{p}}} = [\phi_m^{(1)}, \ldots, \phi_m^{(n_{\mathrm{p}})}] \in \mathbb{C}^{1\times n_{\mathrm{p}}}$ and $\|\boldsymbol{\phi}_m^{n_{\mathrm{p}}}\|^2 = 1$, where $\|\cdot\|$ represents the Euclidean norm of a vector. During the uplink pilot training phase, we can derive the received signal matrix, denoted by $\boldsymbol{Y}_k^{n_{\mathrm{p}}} \in \mathbb{C}^{N_{\mathrm{T}}\times n_{\mathrm{p}}}$, at AP k for transmitting n_{p} pilot

data blocks from $K_{\rm u}$ mobile devices as follows:

$$\boldsymbol{Y}_k^{n_{\rm p}} = \sum_{m=1}^{K_{\rm u}} \sqrt{n_{\rm p}\mathcal{P}_{\rm p}}\boldsymbol{h}_{k,m}\boldsymbol{\phi}_m^{n_{\rm p}} + \boldsymbol{W}_{{\rm p},k} \tag{2}$$

where $\mathcal{P}_{\rm p}$ is the uplink pilot transmit power at the mobile devices and $\boldsymbol{W}_{{\rm p},k} \in \mathbb{C}^{N_{\rm T}\times n_{\rm p}}$ is the AWGN matrix with zero mean and covariance $\mathbf{I}_{N_{\rm T}}$. Then, by projecting the received signal $\boldsymbol{Y}_k^{n_{\rm p}}$ onto $\boldsymbol{\phi}_m^{n_{\rm p}}$, we can obtain the following equation:

$$\begin{aligned}\widetilde{\boldsymbol{y}}_k^{n_{\rm p}} &= \boldsymbol{Y}_k^{n_{\rm p}}\left(\boldsymbol{\phi}_m^{n_{\rm p}}\right)^H \\ &= \sqrt{n_{\rm p}\mathcal{P}_{\rm p}}\boldsymbol{h}_{k,m} + \sum_{\substack{m'=1\\ m'\neq m}}^{K_{\rm u}} \sqrt{n_{\rm p}\mathcal{P}_{\rm p}}\boldsymbol{h}_{k,m'}\left(\boldsymbol{\phi}_m^{n_{\rm p}}\right)^H\boldsymbol{\phi}_{m'}^{n_{\rm p}} + \widetilde{\boldsymbol{w}}_{{\rm p},k}\end{aligned} \tag{3}$$

where $(\cdot)^H$ is the conjugate-transpose of a matrix and $\widetilde{\boldsymbol{w}}_{{\rm p},k} \triangleq \boldsymbol{W}_{{\rm p},k}(\boldsymbol{\phi}_m^{n_{\rm p}})^H$ is an independent and identically distributed (i.i.d.) Gaussian vector with zero mean and covariance $\mathbf{I}_{N_{\rm T}}$. Define $\mathbf{R}_{\mathbf{h}_{k,m}} \triangleq \mathbb{E}[\mathbf{h}_{k,m}(\mathbf{h}_{k,m})^H]$ as the covariance matrix of $\mathbf{h}_{k,m}$, where $\mathbb{E}[\cdot]$ is the expectation operation. Applying the minimum mean-squared error (MMSE) estimator of $\mathbf{h}_{k,m}$ based on the observation of $\widetilde{\boldsymbol{y}}_k^{n_{\rm p}}$, we can obtain the estimated channel's impulse response matrix, denoted by $\widehat{\boldsymbol{h}}_{k,m}$, between AP k and mobile user m as follows:

$$\begin{aligned}\widehat{\boldsymbol{h}}_{k,m} &= \mathbb{E}\left[\mathbf{h}_{k,m}|\widetilde{\boldsymbol{y}}_k^{n_{\rm p}}\right] \\ &= \mathbf{R}_{\mathbf{h}_{k,m},\widetilde{\boldsymbol{y}}_k^{n_{\rm p}}}\left(\mathbf{R}_{\widetilde{\boldsymbol{y}}_k^{n_{\rm p}}}\right)^{-1}\left(\widetilde{\boldsymbol{y}}_k^{n_{\rm p}} - \mathbb{E}\left[\widetilde{\boldsymbol{y}}_k^{n_{\rm p}}\right]\right) + \mathbb{E}\left[\mathbf{h}_{k,m}\right]\end{aligned} \tag{4}$$

where $\mathbf{R}_{\mathbf{h}_{k,m},\widetilde{\boldsymbol{y}}_k^{n_{\rm p}}}$ and $\mathbf{R}_{\widetilde{\boldsymbol{y}}_k^{n_{\rm p}}}$ represent the covariance matrices given as follows:

$$\begin{cases}\mathbf{R}_{\mathbf{h}_{k,m},\widetilde{\boldsymbol{y}}_k^{n_{\rm p}}} = \mathbb{E}\left[\mathbf{h}_{k,m}\left(\widetilde{\boldsymbol{y}}_k^{n_{\rm p}}\right)^H\right] = \sqrt{n_{\rm p}\mathcal{P}_{\rm p}}\mathbf{R}_{\mathbf{h}_{k,m}}; \\ \mathbf{R}_{\widetilde{\boldsymbol{y}}_k^{n_{\rm p}}} = \mathbb{E}\left[\widetilde{\boldsymbol{y}}_k^{n_{\rm p}}\left(\widetilde{\boldsymbol{y}}_k^{n_{\rm p}}\right)^H\right] = n_{\rm p}\mathcal{P}_{\rm p}\mathbf{R}_{\mathbf{h}_{k,m}} + \mathbf{I}_{N_{\rm T}}.\end{cases} \tag{5}$$

Since $\mathbb{E}[\widetilde{\boldsymbol{y}}_k^{n_{\rm p}}]$ and $\mathbb{E}[\mathbf{h}_{k,m}]$ are equal to zero, we have

$$\widehat{\boldsymbol{h}}_{k,m} = \sqrt{n_{\rm p}\mathcal{P}_{\rm p}}\mathbf{R}_{\mathbf{h}_{k,m}}\left(n_{\rm p}\mathcal{P}_{\rm p}\mathbf{R}_{\mathbf{h}_{k,m}} + \mathbf{I}_{N_{\rm T}}\right)^{-1}\widetilde{\boldsymbol{y}}_k^{n_{\rm p}}. \tag{6}$$

B. Downlink Energy Harvesting Model in the Finite Blocklength Regime

We can derive the harvested energies, denoted by $E_m^{\rm TS}$ and $E_m^{\rm PS}$, for TS and PS receivers at mobile device m, respectively, during the downlink SWIPT phase as follows:

$$\begin{cases}E_m^{\rm TS} = \alpha n_{\rm d}T_s\mathcal{P}_{\rm d}\zeta\left|\sum\limits_{k=1}^{K_{\rm a}}\sum\limits_{m'=1}^{K_{\rm u}}\sqrt{\eta_{k,m'}}\left(\widehat{\boldsymbol{h}}_{k,m'}\right)^H\boldsymbol{h}_{k,m}\right|; \\ E_m^{\rm PS} = n_{\rm d}T_s\mathcal{P}_{\rm d}\rho\zeta\left|\sum\limits_{k=1}^{K_{\rm a}}\sum\limits_{m'=1}^{K_{\rm u}}\sqrt{\eta_{k,m'}}\left(\widehat{\boldsymbol{h}}_{k,m'}\right)^H\boldsymbol{h}_{k,m}\right|,\end{cases} \tag{7}$$

where $\zeta \in (0,1)$ is the energy conversion efficiency, T_s is the duration of each channel use, and $\mathcal{P}_{\rm d}$ is the power for downlink transmission at the APs. Observing from Eq. (7), in addition to the channel gain, the amount of harvested energy depends on the PS and TS factors ρ and α. Then, we can derive the total harvested energy, denoted by E_m, for the joint TS-PS protocol at mobile device m during the downlink SWIPT phase as follows:

$$E_m = E_m^{\rm TS} + (1-\alpha)E_m^{\rm PS}. \tag{8}$$

The charging state of battery,denoted by B_m, at mobile device m before the next uplink information transmission phase is given by

$$B_m = \min\left\{B_{\max}, E_m\right\} \tag{9}$$

where $B_{\max}$ is the pre-defined maximum storable energy at the mobile device. Then, the remaining energy, denoted by $E_{{\rm r},m}$, at mobile device m for the next uplink data transmission phase is derived as follows:

$$E_{{\rm r},m} = B_m - (1-\alpha)n_{\rm d}T_s\mathcal{P}_c \tag{10}$$

where $\mathcal{P}_c$ is the circuit and baseband processing power consumption. Without loss of generality, we assume that $\mathcal{P}_c$ is a constant. If the harvested energy during the downlink SWIPT phase is insufficient for the next uplink data transmission, there will be an outage, resulting in data transmission failure. Otherwise, all the remaining energy will be used for data transmissions in the next phase.

C. Downlink Data Transmission in the Finite Blocklength Regime

1) Wireless Downlink Data Transmission Model: Denote by $\widetilde{n}_{\rm d} = (1-\alpha)n_{\rm d}$ the downlink data blocklength during the downlink information transfer sub-phase. We define the transmit signal matrix as $\boldsymbol{X}_k^{\widetilde{n}_{\rm d}} \triangleq [\boldsymbol{x}_k^{(1)},\ldots,\boldsymbol{x}_k^{(\widetilde{n}_{\rm d})}]$ at AP k for transmitting $\widetilde{n}_{\rm d}$ data blocks where $\boldsymbol{x}_k^{(l)}$ $(l=1,\ldots,\widetilde{n}_{\rm d})$ is the transmit signal vector for the lth data block. Define receive signal vector as $\boldsymbol{y}_{{\rm d},m}^{\widetilde{n}_{\rm d}} \triangleq [y_{{\rm d},m}^{(1)},\ldots,y_{{\rm d},m}^{(\widetilde{n}_{\rm d})}]$ at mobile device m. Based on the MMSE estimator $\widehat{\boldsymbol{h}}_{k,m}$, we can derive the transmitted signal with length $\widetilde{n}_{\rm d}$ at AP k by employing conjugate beamforming [31] as follows:

$$\boldsymbol{X}_k^{\widetilde{n}_{\rm d}} = \sqrt{(1-\rho)\mathcal{P}_{\rm d}}\sum_{m=1}^{K_{\rm u}}\sqrt{\eta_{k,m}}\boldsymbol{b}_{k,m}\boldsymbol{s}_m^{\widetilde{n}_{\rm d}} \tag{11}$$

where $\boldsymbol{s}_m^{\widetilde{n}_{\rm d}}$ represents the transmitted signal vector for mobile device m, $\boldsymbol{b}_{k,m} \in \mathbb{C}^{N_{\rm T}\times 1}$ is the precoder vector that AP k assigns to mobile users m, which is given as follows:

$$\boldsymbol{b}_{k,m} = \frac{\widehat{\boldsymbol{h}}_{k,m}}{\sqrt{\mathbb{E}\left[\left\|\widehat{\boldsymbol{h}}_{k,m}\right\|^2\right]}} \tag{12}$$

and $\eta_{k,m}$ is the downlink power allocation coefficient for transmitting from AP k to mobile device m, which is chosen to satisfy the following power constraint at each AP:

$$\sum_{m=1}^{K_{\rm u}}\eta_{k,m}\nu_{k,m} \leq 1 \tag{13}$$

where

$$\nu_{k,m} \triangleq \mathbb{E}\left[\left|\widehat{\boldsymbol{h}}_{k,m}\right|^2\right]. \tag{14}$$

Then, we can derive the received downlink signal, denoted by $\boldsymbol{y}_{\mathrm{d},m}^{\widetilde{n}_{\mathrm{d}}}$, at the mth mobile device as follows:

$$\begin{aligned}\boldsymbol{y}_{\mathrm{d},m}^{\widetilde{n}_{\mathrm{d}}} &= \sum_{k=1}^{K_{\mathrm{a}}} (\boldsymbol{h}_{k,m})^H \boldsymbol{X}_k^{\widetilde{n}_{\mathrm{d}}} + \boldsymbol{w}_{\mathrm{d},m}^{\widetilde{n}_{\mathrm{d}}} \\ &= \sqrt{(1-\rho)\mathcal{P}_{\mathrm{d}}} \sum_{k=1}^{K_{\mathrm{a}}} \sqrt{\eta_{k,m}} (\boldsymbol{h}_{k,m})^H \boldsymbol{h}_{k,m} \boldsymbol{s}_m^{\widetilde{n}_{\mathrm{d}}} + \sqrt{(1-\rho)\mathcal{P}_{\mathrm{d}}} \\ &\quad \times \sum_{k=1}^{K_{\mathrm{a}}} \left[\sum_{\substack{m'=1 \\ m' \neq m}}^{K_{\mathrm{u}}} \sqrt{\eta_{k,m'}} (\boldsymbol{h}_{k,m'})^H \boldsymbol{h}_{k,m} \boldsymbol{s}_{m'}^{\widetilde{n}_{\mathrm{d}}} \right] + \boldsymbol{w}_{\mathrm{d},m}^{\widetilde{n}_{\mathrm{d}}} \end{aligned} \tag{15}$$

where $\boldsymbol{s}_m^{\widetilde{n}_{\mathrm{d}}}$ and $\boldsymbol{s}_{m'}^{\widetilde{n}_{\mathrm{d}}}$ are the signals sent to mobile device m and mobile device m', respectively; $\eta_{k,m}$ and $\eta_{k,m'}$ are the downlink power allocation coefficients for transmitting from AP k to mobile device m and mobile device m', respectively; and $\boldsymbol{w}_{\mathrm{d},m}^{\widetilde{n}_{\mathrm{d}}}$ is the AWGN with zero mean and unit variance at mobile device m. Correspondingly, we can derive the downlink signal-to-noise radio (SNR), denoted by $\gamma_{\mathrm{d},m}$, at mobile device m as follows:

$$\begin{aligned}\gamma_{\mathrm{d},m} &= (1-\rho)\mathcal{P}_{\mathrm{d}} \left| \mathbb{E}\left[\sum_{k=1}^{K_{\mathrm{a}}} \sqrt{\eta_{k,m}} (\boldsymbol{h}_{k,m})^H \boldsymbol{b}_{k,m} \right] \right|^2 \\ &\quad \times \left\{ (1-\rho)\mathcal{P}_{\mathrm{d}} \sum_{m'=1}^{K_{\mathrm{u}}} \mathbb{E}\left[\left| \sum_{k=1}^{K_{\mathrm{a}}} \sqrt{\eta_{k,m'}} (\boldsymbol{h}_{k,m'})^H \boldsymbol{b}_{k,m} \right|^2 \right] \right. \\ &\quad \left. - (1-\rho)\mathcal{P}_{\mathrm{d}} \left| \mathbb{E}\left[\sum_{k=1}^{K_{\mathrm{a}}} \sqrt{\eta_{k,m}} (\boldsymbol{h}_{k,m})^H \boldsymbol{b}_{k,m} \right] \right|^2 + 1 \right\}^{-1}. \end{aligned} \tag{16}$$

Note that the SNR function given in Eq. (16) can be used to investigate the system performance for both TS and PS protocols. By setting $\alpha \neq 0$ and $\rho = 0$, we can derive the SNR function for the TS protocol. On the other hand, setting $\alpha = 0$ and $\rho \neq 0$, we can derive the SNR function for the PS protocol. When $\alpha \neq 0$ and $\rho \neq 0$, Eq. (16) can be used to characterize the SNR for a joint TS-PS protocol.

2) Channel Coding Rate in the Finite Blocklength Regime: We define a message set $\mathcal{M} = \{1, \ldots, M\}$ and a message ω is uniformly distributed on $\mathcal{M}$, where M is the number of codewords. Denote by $\epsilon_{\mathrm{d},m}$ is the downlink decoding error probability for mobile device m. Correspondingly, we define an $(\widetilde{n}_{\mathrm{d}}, M, \epsilon_{\mathrm{d},m})$-code as follows:

- An encoder Υ: $\{1, \ldots, M\} \mapsto \mathbb{C}^{\widetilde{n}_{\mathrm{d}}}$ that maps the message $\omega \in \{1, \ldots, M\}$ into a codeword with length $\widetilde{n}_{\mathrm{d}}$.
- A decoder $\mathcal{D}$: $\mathbb{C}^{\widetilde{n}_{\mathrm{d}}} \mapsto \{1, \ldots, M\}$ that decodes the received message into $\widehat{\omega}$, where $\widehat{\omega}$ denotes the estimated received signal at the receiver. The decoder $\mathcal{D}$ need to satisfy the following maximum error probability constraint:

$$\Pr\{\widehat{\omega} \neq \omega\} \leq \epsilon_{\mathrm{d},m}. \tag{17}$$

Traditionally, Shannon's second theorem generally requires infinite blocklength for attaining the maximum achievable data transmission rate. However, as noted above, with limited bandwidth and stringent delay-bounded QoS constraints in supporting mURLLC services, Shannon's capacity formula cannot be applied for our proposed SWIPT-enabled CF m-MIMO based 6G wireless networks. Towards this end, we can derive the accurate approximation of the maximum achievable downlink coding rate, denoted by $R_{\mathrm{d},m}$, in bits per channel use with decoding error probability $\epsilon_{\mathrm{d},m}$ $(0 \leq \epsilon_{\mathrm{d},m} < 1)$ and coding blocklength $(1-\alpha)n_{\mathrm{d}}$ for mobile device m in the finite blocklength regime as follows [16]:

$$R_{\mathrm{d},m} \approx C(\gamma_{\mathrm{d},m}) - \sqrt{\frac{V(\gamma_{\mathrm{d},m})}{(1-\alpha)n_{\mathrm{d}}}} Q^{-1}(\epsilon_{\mathrm{d},m}) \tag{18}$$

where $Q^{-1}(\cdot)$ is the inverse of Q-function, $\gamma_{\mathrm{d},m}$ represents the SNR at mobile device m, and $C(\gamma_{\mathrm{d},m})$ and $V(\gamma_{\mathrm{d},m})$ are the downlink channel capacity and channel dispersion, respectively, at mobile device m, which are given in the following equations:

$$\begin{cases} C(\gamma_{\mathrm{d},m}) = \log_2(1+\gamma_{\mathrm{d},m}); \\ V(\gamma_{\mathrm{d},m}) = 1 - \frac{1}{(1+\gamma_{\mathrm{d},m})^2}. \end{cases} \tag{19}$$

III. Downlink ϵ-Effective Capacity and Harvested Energy Tradeoff Optimization for Statistical Delay/Error-Rate Bounded QoS Using FBC

Statistical delay-bounded QoS guarantees [36], [37] have been extensively studied for analyzing queuing behavior for time-varying arrival and service processes. Based on the large deviation principle (LDP), under sufficient conditions, the queue length process, denoted by $Q_m(t)$, converges in distribution to a random variable $Q_m(\infty)$ such that [6]

$$-\lim_{Q_{\mathrm{th}} \to \infty} \frac{\log\left(\Pr\{Q_m(\infty) > Q_{\mathrm{th}}\}\right)}{Q_{\mathrm{th}}} = \theta_m, \tag{20}$$

where $\theta_m > 0$ is defined as the QoS exponent for mobile device m and plays a critically important role for statistical delay-bounded QoS provisioning. Eq. (20) states that the probability of the queue length exceeding a certain threshold Q_{th} decays exponentially fast as the threshold Q_{th} increases. However, the traditional effective capacity theory measures queuing process based on the Shannon's second theorem, which requires infinite blocklength without considering the decoding error at the receiver. For our proposed SWIPT-enabled CF m-MIMO based schemes, we apply the FBC technique which considers both delay and error-rate bounded QoS requirements. As a result, we introduce a new concept of *ϵ-effective capacity* in supporting mURLLC with non-vanishing error probability. We define the downlink ϵ-effective capacity, denoted by $EC_{\mathrm{d},m}^{\epsilon}(\theta_m)$, in the finite blocklength for statistical delay and error-rate bounded QoS provisioning as follows:

$$\begin{aligned} EC_{\mathrm{d},m}^{\epsilon}(\theta_m) \triangleq & -\frac{1}{\theta_m} \log\left\{ \mathbb{E}_{\gamma_{\mathrm{d},m}}\left[\epsilon_{\mathrm{d},m} + (1-\epsilon_{\mathrm{d},m}) \right.\right. \\ & \left.\left. \times e^{-\theta_m(1-\alpha)n_{\mathrm{d}}R_{\mathrm{d},m}} \right] \right\} \end{aligned} \tag{21}$$

where $\mathbb{E}_{\gamma_{\mathrm{d},m}}[\cdot]$ is the expectation with respect to the SNR $\gamma_{\mathrm{d},m}$ and $R_{\mathrm{d},m}$ is the downlink data transmission rate at mobile device m, which is specified by Eq. (18). Note that similar to the SNR in Eq. (16), we can derive the downlink ϵ-effective capacity, denoted by $EC_{\mathrm{d},m}^{\epsilon,\mathrm{TS}}(\theta_m)$, for the TS receiver at mobile device m by setting $\alpha \neq 0$ and $\rho = 0$ in the above Eq. (21). On the other hand, setting $\alpha = 0$ and $\rho \neq 0$ in the above Eq. (21), we can derive the downlink ϵ-effective capacity, denoted by $EC_{\mathrm{d},m}^{\epsilon,\mathrm{PS}}(\theta_m)$, for the PS receiver at mobile device m. When $\alpha \neq 0$ and $\rho \neq 0$, we can derive the downlink ϵ-effective capacity, denoted by $EC_{\mathrm{d},m}^{\epsilon,\text{TS-PS}}(\theta_m)$, a joint TS-PS protocol at mobile device m.

A. TS Protocol

Previous works have shown the optimal transmission strategies for the maximum power transfer and information transfer are in general different [38], [39]. The rate-energy (R-E) tradeoff is a very effective way to fundamentally characterize the performance of SWIPT-enabled schemes. Towards this end, the R-E tradeoff has been extensively studied in the previous literatures considering infinite blocklength using Shannon's second theorem. For our proposed SWIPT-enabled CF m-MIMO based schemes, we apply the FBC technique and characterize the downlink ϵ-effective capacity-energy tradeoff for statistical delay and error-rate bounded QoS provisioning in supporting mURLLC with non-vanishing decoding error probability. There have been a number of works focusing on investigating the rate-energy tradeoff curves for implementing SWIPT technique in the finite blocklength regime to support mURLLC. In particular, the authors of [28] have characterized the fundamental limits of SWIPT in terms of the information-energy capacity region in the non-asymptotic regime. The authors of [29] have investigated the rate-energy tradeoff and the decoding error probability-energy tradeoff for SWIPT systems in the finite blocklength realm. However, the previous research works have not analyzed the information-energy tradeoff by taking into account the statistical delay and error-rate QoS provisioning, which is an importing issue for supporting the mURLLC services. Therefore, we focus on investigating the optimal ϵ-effective capacity-energy tradeoff problems for SWIPT-enabled schemes for statistical delay and error-rate bounded QoS provisioning to support mURLLC with non-vanishing decoding error probability. Considering the case of no power adaptation, Fig. 2 plots the downlink ϵ-effective capacity-energy region for both TS and PS receivers compared with the ideal receiver, which is assumed to be able to decode information and harvest energy from the same signal simultaneously [40], [41]. As shown in Fig. 2, the downlink ϵ-effective capacity-energy region for TS and PS receivers is a concave-shape region. We can observe from Fig. 2 that a PS receiver outperforms a TS receiver in terms of the downlink ϵ-effective capacity-energy tradeoff.

In this paper, we focus on investigating the optimal ϵ-effective capacity-energy tradeoff problems for SWIPT-enabled schemes with power allocation. Thus, taking into account both TS factor and power allocation coefficient, we define the downlink ϵ-effective capacity-energy region, denoted by $\mathcal{C}_{\mathrm{EC}_{\mathrm{d},m}^{\epsilon,\mathrm{TS}}-\mathrm{E}_m^{\mathrm{TS}}}$, under TS protocol for statistical delay and error-rate bounded QoS

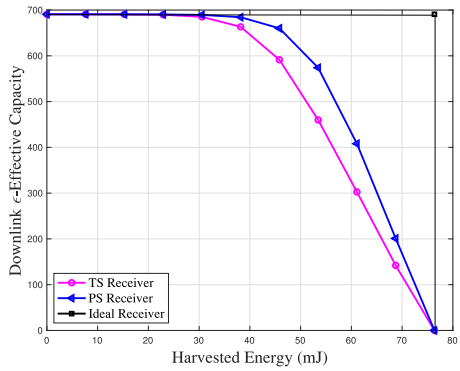

Fig. 2. The downlink ϵ-effective capacity-energy region of different SWIPT receivers for the case of no power adaptation using FBC.

provisioning in the finite blocklength as follows:

$$\mathcal{C}_{\mathrm{EC}_{\mathrm{d},m}^{\epsilon,\mathrm{TS}}-\mathrm{E}_m^{\mathrm{TS}}} \triangleq \bigcup_{\substack{0\le\eta_{k,m}\le 1,\forall k \\ 0\le\alpha\le 1}} \left\{ \left(EC_{\mathrm{d},m}^{\epsilon,\mathrm{TS}}, E_m^{\mathrm{TS}} \right) : EC_{\mathrm{d},m}^{\epsilon,\mathrm{TS}} \le -\frac{1}{\theta_m} \times \log\left\{ \mathbb{E}_{\gamma_{\mathrm{d},m}}\left[\epsilon_{\mathrm{d},m} + (1-\epsilon_{\mathrm{d},m})\, e^{-\theta_m(1-\alpha)n_{\mathrm{d}}T_s R_{\mathrm{d},m}} \right] \right\}, \right.$$
$$\left. E_m^{\mathrm{TS}} \le \alpha n_{\mathrm{d}} T_s \mathcal{P}_{\mathrm{d}} \zeta \left| \sum_{k=1}^{K_{\mathrm{a}}} \sum_{m'=1}^{K_{\mathrm{u}}} \sqrt{\eta_{k,m'}} \left(\widehat{\boldsymbol{h}}_{k,m'} \right)^H \boldsymbol{h}_{k,m} \right| \right\}. \tag{22}$$

Since the optimal tradeoff between the maximum downlink ϵ-effective capacity and harvested energy is characterized by the boundary of the downlink ϵ-effective capacity-energy region, it is important to characterize all the boundary pairs of downlink ϵ-effective capacity and harvested energy. We can formulate the following optimization problem for our proposed SWIPT-enabled CF m-MIMO based schemes to obtain the boundaries of downlink ϵ-effective capacity-energy region under TS protocol in the finite blocklength regime:

$$\mathbf{P_1}: \arg \max_{\{\alpha, n_{\mathrm{d}}, \eta_{k,m}, \forall m,k\}} \left\{ \sum_{m=1}^{K_u} EC_{\mathrm{d},m}^{\epsilon,\mathrm{TS}}(\theta_m) \right\} \tag{23}$$

$$\text{s.t. } C1: E_m^{\mathrm{TS}} \ge \overline{E}_{\min}; \tag{24}$$

$$C2: \sum_{m=1}^{K_{\mathrm{u}}} \eta_{k,m}\nu_{k,m} \le 1; \tag{25}$$

$$C3: 0 < \alpha < 1, \tag{26}$$

where $\overline{E}_{\min}$ is the minimum required harvested energy. Then, we can convert $\mathbf{P_1}$ into the following equivalent minimization problem:

$$\mathbf{P_2}: \arg \min_{\{\alpha, n_{\mathrm{d}}, \eta_{k,m}, \forall m,k\}} \left\{ \sum_{m=1}^{K_u} \mathbb{E}_{\gamma_{\mathrm{d},m}} \left[\epsilon_{\mathrm{d},m} + (1-\epsilon_{\mathrm{d},m}) \exp\left\{ -\theta_m \times (1-\alpha) n_{\mathrm{d}} T_s R_{\mathrm{d},m} \right\} \right] \right\} \tag{27}$$

subject to the same constraints C1, C2, and C3 given by Eqs. (24), (25), and (26), respectively. The optimization problem $\mathbf{P_2}$ given by Eq. (27) is challenging in terms of finding the global optimal solution due to highly-coupling among variables. To overcome such issue, an alternative optimization technique can be developed in an efficient manner where an improved solution is obtained at each step of iteration with guaranteed convergence by applying the successive convex approximation (SCA) techniques. By using the SCA techniques, we do not need to characterize the joint convexity across all variables, and instead, we can only characterize the convexity for each given individual variable when fixing the other variables in our proposed optimization problems to make the complexity-analysis problem feasible. Therefore, to solve the optimization problem $\mathbf{P_2}$ specified by Eq. (27), we characterize the convexity of the objective function in $\mathbf{P_2}$ as detailed in the following theorem.

Theorem 1: **If** the harvested energy E_m^{TS} is characterized by Eq. (7), **then** the following claims hold for our proposed SWIPT-enabled CF m-MIMO based schemes in supporting statistical delay and error-rate bounded QoS provisioning under TS protocol in the finite blocklength regime.

Claim 1. Given fixed downlink power allocation coefficient $\eta_{k,m}$ and downlink data blocklength n_{d}, the objective function in $\mathbf{P_2}$ is *convex* in α when $\epsilon_{\mathrm{d},m} \in (0, 0.5)$ and $n_{\mathrm{d}} > n_{\mathrm{d,th}}^{\mathrm{TS}}$, where

$$n_{\mathrm{d,th}}^{\mathrm{TS}} \triangleq \frac{1}{(1-\alpha)} \left[\frac{Q^{-1}(\epsilon_{\mathrm{d},m})}{C\left(\gamma_{\mathrm{d},m}\right) - \frac{C(\gamma_{\mathrm{d},m})}{4(1-\alpha)\theta_m n_{\mathrm{d}} T_s C(\gamma_{\mathrm{d},m})+1}} \right]^2. \tag{28}$$

Claim 2. Given fixed TS factor α and downlink power allocation coefficient $\eta_{k,m}$, the objective function in $\mathbf{P_2}$ is *convex* in n_{d} when $\epsilon_{\mathrm{d},m} \in (0, 0.5)$.

Claim 3. Given fixed TS factor α and downlink data blocklength n_{d}, the objective function in $\mathbf{P_2}$ is *convex* in $\eta_{k,m}$ when $\epsilon_{\mathrm{d},m} \in (0, 0.5)$.

Proof: We proceed with the proof by showing Claim 1, Claim 2, and Claim 3, respectively.

Claim 1. To characterize the convexity of the objective function in $\mathbf{P_2}$ given by Eq. (27) with respect to the TS factor α, first we define two auxiliary functions as follows:

$$\begin{cases} F\left(\gamma_{\mathrm{d},m}\right) \triangleq \mathbb{E}_{\gamma_{\mathrm{d},m}}\left[\epsilon_{\mathrm{d},m} + (1-\epsilon_{\mathrm{d},m})\, e^{-\theta_m (1-\alpha) n_{\mathrm{d}} T_s R_{\mathrm{d},m}}\right]; \\ F_1(\gamma_{\mathrm{d},m}) \triangleq (1-\alpha) R_{\mathrm{d},m} \\ \qquad\qquad = (1-\alpha) C\left(\gamma_{\mathrm{d},m}\right) - \sqrt{\frac{(1-\alpha)V(\gamma_{\mathrm{d},m})}{n_{\mathrm{d}}}} Q^{-1}(\epsilon_{\mathrm{d},m}). \end{cases} \tag{29}$$

Thus, we have

$$F\left(\gamma_{\mathrm{d},m}\right) = \mathbb{E}_{\gamma_{\mathrm{d},m}}\left[\epsilon_{\mathrm{d},m} + (1-\epsilon_{\mathrm{d},m})\, e^{-\theta_m n_{\mathrm{d}} T_s F_1(\gamma_{\mathrm{d},m})}\right]. \tag{30}$$

Second, we can derive the first-order derivative of the auxiliary function $F(\gamma_{\mathrm{d},m})$ with respect to the TS factor α as in the following equation:

$$\frac{\partial F\left(\gamma_{\mathrm{d},m}\right)}{\partial \alpha} = \frac{\partial F\left(\gamma_{\mathrm{d},m}\right)}{\partial F_1(\gamma_{\mathrm{d},m})} \frac{\partial F_1(\gamma_{\mathrm{d},m})}{\partial \alpha} \tag{31}$$

where

$$\frac{\partial F\left(\gamma_{\mathrm{d},m}\right)}{\partial F_1(\gamma_{\mathrm{d},m})} = \mathbb{E}_{\gamma_{\mathrm{d},m}}\left[-(1-\epsilon_{\mathrm{d},m})\, e^{-\theta_m (1-\alpha) n_{\mathrm{d}} T_s R_{\mathrm{d},m}} \theta_m n_{\mathrm{d}} T_s \right] < 0 \tag{32}$$

and

$$\frac{\partial F_1(\gamma_{\mathrm{d},m})}{\partial \alpha} = -C\left(\gamma_{\mathrm{d},m}\right) + \sqrt{\frac{V\left(\gamma_{\mathrm{d},m}\right)}{n_{\mathrm{d}}}} \frac{Q^{-1}(\epsilon_{\mathrm{d},m})\,(1-\alpha)^{-\frac{1}{2}}}{2}. \tag{33}$$

Third, using chain rule, we derive the second-order derivative of $F(\gamma_{\mathrm{d},m})$ with respect to the TS factor α as follows:

$$\frac{\partial^2 F\left(\gamma_{\mathrm{d},m}\right)}{\partial \alpha^2} = \frac{\partial^2 F\left(\gamma_{\mathrm{d},m}\right)}{\partial \left[F_1(\gamma_{\mathrm{d},m})\right]^2} \left[\frac{\partial F_1(\gamma_{\mathrm{d},m})}{\partial \alpha}\right]^2 + \frac{\partial F\left(\gamma_{\mathrm{d},m}\right)}{\partial F_1(\gamma_{\mathrm{d},m})} \times \frac{\partial^2 F_1(\gamma_{\mathrm{d},m})}{\partial \alpha^2} \tag{34}$$

where

$$\frac{\partial^2 F\left(\gamma_{\mathrm{d},m}\right)}{\partial \left[F_1(\gamma_{\mathrm{d},m})\right]^2} = \mathbb{E}_{\gamma_{\mathrm{d},m}}\left[(1-\epsilon_{\mathrm{d},m})\, e^{-\theta_m (1-\alpha) n_{\mathrm{d}} T_s R_{\mathrm{d},m}} \times \left(\theta_m n_{\mathrm{d}} T_s\right)^2 \right] > 0 \tag{35}$$

and

$$\frac{\partial^2 F_1(\gamma_{\mathrm{d},m})}{\partial \alpha^2} = \sqrt{\frac{V\left(\gamma_{\mathrm{d},m}\right)}{n_{\mathrm{d}}}} \frac{Q^{-1}(\epsilon_{\mathrm{d},m})\,(1-\alpha)^{-\frac{3}{2}}}{4}. \tag{36}$$

Since when $Q^{-1}(\epsilon_{\mathrm{d},m}) > 0$ for $\epsilon_{\mathrm{d},m} \in (0, 0.5)$, we can obtain $\partial^2 F_1(\gamma_{\mathrm{d},m})/\partial \alpha^2 > 0$. The proof for showing $\partial^2 F\left(\gamma_{\mathrm{d},m}\right)/\partial \alpha^2 > 0$ when $\epsilon_{\mathrm{d},m} \in (0, 0.5)$ and $n_{\mathrm{d}} > n_{\mathrm{d,th}}^{\mathrm{TS}}$ is given in Appendix B. Therefore, the objective function in $\mathbf{P_2}$ specified by Eq. (27) is convex with respect to the TS factor α when $\epsilon_{\mathrm{d},m} \in (0, 0.5)$ and the constraint $n_{\mathrm{d}} > n_{\mathrm{d,th}}^{\mathrm{TS}}$ is satisfied, which completes the proof of Claim 1 in Theorem 1.

Claim 2. To characterize the convexity of the objective function in $\mathbf{P_2}$ given by Eq. (27) with respect to the downlink data blocklength n_{d}, first we define the auxiliary function, denoted by $F_2(\gamma_{\mathrm{d},m})$, as follows:

$$F_2(\gamma_{\mathrm{d},m}) \triangleq n_{\mathrm{d}} R_{\mathrm{d},m} = n_{\mathrm{d}} C\left(\gamma_{\mathrm{d},m}\right) - \sqrt{\frac{n_{\mathrm{d}} V\left(\gamma_{\mathrm{d},m}\right)}{1-\alpha}} Q^{-1}(\epsilon_{\mathrm{d},m}). \tag{37}$$

Second, we derive the first-order derivative of the auxiliary function $F(\gamma_{\mathrm{d},m})$ with respect to the downlink data blocklength n_{d} as follows:

$$\frac{\partial F\left(\gamma_{\mathrm{d},m}\right)}{\partial n_{\mathrm{d}}} = \frac{\partial F\left(\gamma_{\mathrm{d},m}\right)}{\partial F_2(\gamma_{\mathrm{d},m})} \frac{\partial F_2(\gamma_{\mathrm{d},m})}{\partial n_{\mathrm{d}}} \tag{38}$$

where

$$\frac{\partial F\left(\gamma_{\mathrm{d},m}\right)}{\partial F_2(\gamma_{\mathrm{d},m})} = \mathbb{E}_{\gamma_{\mathrm{d},m}}\left[-(1-\epsilon_{\mathrm{d},m})\, e^{-\theta_m (1-\alpha) n_{\mathrm{d}} T_s R_{\mathrm{d},m}} \theta_m \times (1-\alpha) T_s \right] < 0 \tag{39}$$

and

$$\frac{\partial F_2(\gamma_{\mathrm{d},m})}{\partial n_{\mathrm{d}}} = C\left(\gamma_{\mathrm{d},m}\right) - \sqrt{\frac{V\left(\gamma_{\mathrm{d},m}\right)}{1-\alpha}}\frac{Q^{-1}(\epsilon_{\mathrm{d},m})\left(n_{\mathrm{d}}\right)^{-\frac{1}{2}}}{2}. \tag{40}$$

Third, using chain rule, we derive the second-order derivative of $F(\gamma_{\mathrm{d},m})$ with respect to n_{d} as follows:

$$\frac{\partial^2 F\left(\gamma_{\mathrm{d},m}\right)}{\partial (n_{\mathrm{d}})^2} = \frac{\partial^2 F\left(\gamma_{\mathrm{d},m}\right)}{\partial\left[F_2(\gamma_{\mathrm{d},m})\right]^2}\left[\frac{\partial F_2(\gamma_{\mathrm{d},m})}{\partial n_{\mathrm{d}}}\right]^2 + \frac{\partial F\left(\gamma_{\mathrm{d},m}\right)}{\partial F_2(\gamma_{\mathrm{d},m})} \times \frac{\partial^2 F_2(\gamma_{\mathrm{d},m})}{\partial (n_{\mathrm{d}})^2} \tag{41}$$

where

$$\frac{\partial^2 F\left(\gamma_{\mathrm{d},m}\right)}{\partial\left[F_2(\gamma_{\mathrm{d},m})\right]^2} = \mathbb{E}_{\gamma_{\mathrm{d},m}}\Big[\left(1-\epsilon_{\mathrm{d},m}\right)e^{-\theta_m(1-\alpha)n_{\mathrm{d}}T_s R_{\mathrm{d},m}} \times \left[\theta_m(1-\alpha)T_s\right]^2\Big] > 0 \tag{42}$$

and

$$\frac{\partial^2 F_2(\gamma_{\mathrm{d},m})}{\partial (n_{\mathrm{d}})^2} = -\sqrt{\frac{V\left(\gamma_{\mathrm{d},m}\right)}{1-\alpha}}\frac{Q^{-1}(\epsilon_{\mathrm{d},m})\left(n_{\mathrm{d}}\right)^{-\frac{3}{2}}}{4}. \tag{43}$$

Since when $Q^{-1}(\epsilon_{\mathrm{d},m}) > 0$ for $\epsilon_{\mathrm{d},m} \in (0, 0.5)$, we can obtain $\partial^2 F_2(\gamma_{\mathrm{d},m})/\partial(n_{\mathrm{d}})^2 > 0$. Therefore, we can obtain $\partial^2 F\left(\gamma_{\mathrm{d},m}\right)/\partial(n_{\mathrm{d}})^2 > 0$, implying that the objective function in $\mathbf{P_2}$ specified by Eq. (27) is convex with respect to the downlink data blocklength n_{d} when $\epsilon_{\mathrm{d},m} \in (0, 0.5)$, which completes the proof of Claim 2 in Theorem 1.

Claim 3. Similar to the proof of Claim 2, we can easily show that the second-order derivative $\partial^2 F\left(\gamma_{\mathrm{d},m}\right)/\partial(\eta_{k,m})^2 > 0$, implying that the objective function in $\mathbf{P_2}$ specified by Eq. (27) is convex with respect to the downlink power allocation coefficient $\eta_{k,m}$ when $\epsilon_{\mathrm{d},m} \in (0, 0.5)$. Thus, we complete the proof of Claim 3 in Theorem 1. ■

Remarks on Theorem 1: Theorem 1 implies that there exists a local optimal solution to the minimization problem $\mathbf{P_2}$ given by Eq. (27) when the other two variables are fixed. Therefore, the minimization problem $\mathbf{P_2}$ can be efficiently solved by applying the SCA techniques with an iterative search method. In particular, we start with the initialized values of the TS factor, denoted by $\alpha^{(0)}$, downlink data blocklength, denoted by $n_{\mathrm{d}}^{(0)}$, and downlink power allocation coefficient, denoted by $\eta_{k,m}^{(0)}$. In Step 1, we formulate a local problem aiming at minimizing the objective function in $\mathbf{P_2}$ given by Eq. (27) over n_{d}. We solve this local minimization problem and determine the optimal downlink data blocklength, denoted by $n_{\mathrm{d}}^{\mathrm{opt}}$, to $\mathbf{P_2}$. In Step 2, based on $n_{\mathrm{d}}^{\mathrm{opt}}$, we repeat the same process for new local problem to minimize the objective function in $\mathbf{P_2}$ given by Eq. (27) over the TS factor α. In Step 3, based on $n_{\mathrm{d}}^{\mathrm{opt}}$ and α derived in the previous Step 1 and Step 2, we repeat the same process to solve the local problem to minimize the objective function in $\mathbf{P_2}$ over $\eta_{k,m}$. We repeat Step 1–Step 3 until the solution converges. We define $n_{\mathrm{d}}^{(\ell)}$, $\alpha^{(\ell)}$, and $\eta_{k,m}^{(\ell)}$ as the downlink blocklength, TS factor, and downlink power allocation coefficient in the ℓth iteration ($\ell = 0, 1, 2, \ldots$), respectively. We develop an iterative algorithm as shown in **Algorithm 1** to solve the optimization problem $\mathbf{P_2}$ for our proposed SWIPT-enabled CF m-MIMO based schemes under TS protocol in the finite blocklength regime. To analyze the convergence of the above **Algorithm 1**, it is easy to show that the optimal value of each local problem is definitely not lower than the optimal value of the original problem given by Eq. (27). According to [33], the convergence of **Algorithm 1** is therefore guaranteed, i.e., at least a local optimal solution can be achieved. Note that according to Theorem 1, the objective function in $\mathbf{P_2}$ is smooth and differentiable in $\{\alpha, n_{\mathrm{d}}, \eta_{k,m}\}$ in the feasible set, and the objective function in $\mathbf{P_2}$ is convex in α, n_{d}, and $\eta_{k,m}$, respectively, when the other two variables are fixed. Therefore, it is easy to show that the local optimal solution is unique, thus, it is also the global optimal solution.

Algorithm 1: Joint Optimization Algorithm Under TS Protocol for solving $\mathbf{P_2}$ in Eq. (27).

Input: $K_{\mathrm{a}}, K_{\mathrm{u}}, M, n_{\mathrm{p}}, \beta_{k,m}, \mathcal{P}_{\mathrm{p}}, \mathcal{P}_{\mathrm{d}}, \theta_m, T_s, \overline{E}_{\min}$
Initialization: $\ell = 0$ and $\{\alpha^{(0)}, n_{\mathrm{d}}^{(0)}, \eta_{k,m}^{(0)}\}$
Repeat
  Step 1:
  Solve $\arg\min_{n_{\mathrm{d}}}\{\sum_{m=1}^{K_u} F(\gamma_{\mathrm{d},m})\}$ in Eq. (27), denote by $n_{\mathrm{d}}^{(\ell+1)}$
if $n_{\mathrm{d}}^{(\ell+1)}$ is an integer **then**
  $n_{\mathrm{d}}^{(\ell+1)} \rightarrow n_{\mathrm{d}}^{\mathrm{opt}}$
else
  $n_{\mathrm{d}}^{(\ell+1)} = \min_{n_{\mathrm{d}} \in \left\{n_{\mathrm{d}}^{\mathrm{floor}}, n_{\mathrm{d}}^{\mathrm{cell}}\right\}}\{\sum_{m=1}^{K_u} F(\gamma_{\mathrm{d},m})\}$, where
  $n_{\mathrm{d}}^{\mathrm{floor}} = \lfloor n_{\mathrm{d}}^{\mathrm{opt}} \rfloor$ and $n_{\mathrm{d}}^{\mathrm{cell}} = \lceil n_{\mathrm{d}}^{\mathrm{opt}} \rceil$
end if
  Step 2:
  Solve $\arg\min_{\alpha}\{\sum_{m=1}^{K_u} F(\gamma_{\mathrm{d},m})\}$ in Eq. (27), denote the solution by $\alpha^{(\ell+2)}$
  Step 3:
  Solve $\arg\min_{\eta_{k,m}, \forall m,k}\{\sum_{m=1}^{K_u} F(\gamma_{\mathrm{d},m})\}$ in Eq. (27), denote the solution by $\eta_{k,m}^{(\ell+3)}$
  $\ell \leftarrow (\ell + 1)$
Repeat Step 1–Step 3 until the solution converges

B. PS Protocol

Considering the PS protocol, we define the downlink ϵ-effective capacity-energy region, denoted by $\mathcal{C}_{\mathrm{EC}_{\mathrm{d},m}^{\epsilon,\mathrm{PS}}-\mathrm{E}_m^{\mathrm{PS}}}$, as follows:

$$\mathcal{C}_{\mathrm{EC}_{\mathrm{d},m}^{\epsilon,\mathrm{PS}}-\mathrm{E}_m^{\mathrm{PS}}} \triangleq \bigcup_{\substack{0\le\eta_{k,m}\le 1,\forall k \\ 0\le\rho\le 1}} \left\{ \left(EC_{\mathrm{d},m}^{\epsilon,\mathrm{PS}}, E_m^{\mathrm{PS}}\right) : EC_{\mathrm{d},m}^{\epsilon,\mathrm{PS}} \le -\frac{1}{\theta_m} \times \log\left\{\mathbb{E}_{\gamma_{\mathrm{d},m}}\left[\epsilon_{\mathrm{d},m} + (1-\epsilon_{\mathrm{d},m})\, e^{-\theta_m n_{\mathrm{d}} T_s R_{\mathrm{d},m}}\right]\right\},$$

$$E_m^{\mathrm{PS}} \leq n_{\mathrm{d}} T_s \mathcal{P}_{\mathrm{d}} \rho \zeta \left| \sum_{k=1}^{K_{\mathrm{a}}} \sum_{m'=1}^{K_{\mathrm{u}}} \sqrt{\eta_{k,m'}} \left(\widehat{\boldsymbol{h}}_{k,m'} \right)^H \boldsymbol{h}_{k,m} \right| \Bigg\}. \tag{44}$$

As a result, we can formulate the following optimization problem for our proposed SWIPT-enabled CF m-MIMO based schemes under PS protocol in the finite blocklength regime:

$$\mathbf{P_3}: \arg \max_{\{\rho, n_{\mathrm{d}}, \eta_{k,m}, \forall m,k\}} \left\{ \sum_{m=1}^{K_u} EC_{\mathrm{d},m}^{\epsilon,\mathrm{PS}}(\theta_m) \right\} \tag{45}$$

$$\text{s.t. } C1, C2;$$

$$C4: 0 < \rho < 1. \tag{46}$$

Then, we can convert $\mathbf{P_3}$ into the following equivalent minimization problem:

$$\mathbf{P_4}: \arg \min_{\{\rho, n_{\mathrm{d}}, \eta_{k,m}, \forall m,k\}} \left\{ \sum_{m=1}^{K_u} \mathbb{E}_{\gamma_{\mathrm{d},m}} \left[\epsilon_{\mathrm{d},m} + (1-\epsilon_{\mathrm{d},m}) e^{-\theta_m n_{\mathrm{d}} T_s R_{\mathrm{d},m}} \right] \right\} \tag{47}$$

subject to the same constraints C1, C2, and C4 given by Eqs. (24), (25) and (46), respectively. Similar to Theorem 1, the optimization problem $\mathbf{P_4}$ given by Eq. (47) is challenging in terms of finding the global optimal solution due to highly-coupling among variables. We apply an alternative optimization technique in an efficient manner where an improved solution is obtained at each step of iteration with guaranteed convergence by applying the SCA techniques. Therefore, to solve the optimization problem $\mathbf{P_4}$ specified by Eq. (47), we need to characterize the convexity of the objective function in $\mathbf{P_4}$ as detailed in the following theorem.

Theorem 2: Given fixed power allocation coefficient $\eta_{k,m}$ and downlink blocklength n_{d}, the objective function in $\mathbf{P_4}$ specified by Eq. (47) is convex in the PS factor ρ for our proposed SWIPT-enabled CF m-MIMO based schemes under PS protocol in the finite blocklength regime when $\epsilon_{\mathrm{d},m} \in (0, 0.5)$ and $n_{\mathrm{d}} > n_{\mathrm{d,th}}^{\mathrm{PS}}$, where

$$n_{\mathrm{d,th}}^{\mathrm{PS}} \triangleq \frac{9}{V(\gamma_{\mathrm{d},m})} \left[\frac{Q^{-1}(\epsilon_{\mathrm{d},m})(\log 2)}{(1+\gamma_{\mathrm{d},m})^2} \right]^2. \tag{48}$$

Proof: To characterize the convexity of the objective function in $\mathbf{P_4}$ specified in Eq. (47) with respect to the PS factor ρ, first we can derive the first-order derivative of the auxiliary function $F(\gamma_{\mathrm{d},m})$ with respect to the PS factor ρ as follows:

$$\frac{\partial F(\gamma_{\mathrm{d},m})}{\partial \rho} = \frac{\partial F(\gamma_{\mathrm{d},m})}{\partial R_{\mathrm{d},m}} \frac{\partial R_{\mathrm{d},m}}{\partial \rho} \tag{49}$$

where

$$\frac{\partial F(\gamma_{\mathrm{d},m})}{\partial R_{\mathrm{d},m}} = \mathbb{E}_{\gamma_{\mathrm{d},m}} \left[-(1-\epsilon_{\mathrm{d},m}) e^{-\theta_m n_{\mathrm{d}} T_s R_{\mathrm{d},m}} \theta_m n_{\mathrm{d}} T_s \right] < 0 \tag{50}$$

and

$$\frac{\partial R_{\mathrm{d},m}}{\partial \rho} = \frac{\partial C(\gamma_{\mathrm{d},m})}{\partial \rho} - \frac{Q^{-1}(\epsilon_{\mathrm{d},m})}{2\sqrt{n_{\mathrm{d}} V(\gamma_{\mathrm{d},m})}} \frac{\partial V(\gamma_{\mathrm{d},m})}{\partial \rho}. \tag{51}$$

Second, using chain rule, we derive the second-order derivative of $F(\gamma_{\mathrm{d},m})$ with respect to the PS factor ρ as follows:

$$\frac{\partial^2 F(\gamma_{\mathrm{d},m})}{\partial \rho^2} = \frac{\partial^2 F(\gamma_{\mathrm{d},m})}{\partial [R_{\mathrm{d},m}]^2} \left[\frac{\partial R_{\mathrm{d},m}}{\partial \rho} \right]^2 + \frac{\partial F(\gamma_{\mathrm{d},m})}{\partial R_{\mathrm{d},m}} \frac{\partial^2 R_{\mathrm{d},m}}{\partial \rho^2} \tag{52}$$

where

$$\frac{\partial^2 F(\gamma_{\mathrm{d},m})}{\partial [R_{\mathrm{d},m}]^2} = (1-\epsilon_{\mathrm{d},m}) (\theta_m n_{\mathrm{d}} T_s)^2 e^{-\theta_m n_{\mathrm{d}} T_s R_{\mathrm{d},m}} > 0. \tag{53}$$

Since $\partial^2 F(\gamma_{\mathrm{d},m}) / \partial [R_{\mathrm{d},m}]^2 > 0$ and $\partial F(\gamma_{\mathrm{d},m}) / \partial R_{\mathrm{d},m} < 0$, to determine whether $\partial^2 F(\gamma_{\mathrm{d},m}) / \partial \rho^2 > 0$ in Eq. (52), it is equivalent to determine whether $\partial^2 R_{\mathrm{d},m} / \partial \rho^2 < 0$. The proof for showing $\partial^2 R_{\mathrm{d},m} / \partial \rho^2 < 0$ when $\epsilon_{\mathrm{d},m} \in (0, 0.5)$ and $n_{\mathrm{d}} > n_{\mathrm{d,th}}^{\mathrm{PS}}$ is given in Appendix C. Therefore, we obtain $\partial^2 F(\gamma_{\mathrm{d},m}) / \partial \rho^2 > 0$, implying that the objective function in $\mathbf{P_4}$ specified by Eq. (47) is convex with respect to the PS factor ρ when $\epsilon_{\mathrm{d},m} \in (0, 0.5)$ and the constraint in Eq. (84) is satisfied, which completes the proof of Theorem 2. ■

Remarks on Theorem 2: Similar to Theorem 1, Theorem 2 implies that there exists a local optimal solution to the minimization problem $\mathbf{P_4}$ given by Eq. (47) when the other two variables are fixed. It is easy to show that the local optimal solution is unique, thus, it is also the global optimal solution. Therefore, $\mathbf{P_4}$ can be efficiently solved by using the similar approach as described in **Algorithm 1**.

IV. Joint Uplink ϵ-Effective Capacity and Harvested Energy Tradeoff for Statistical Delay and Error-Rate Bounded QoS Using FBC

A. Uplink Data Transmission in the Finite Blocklength Regime

During the uplink data transmission phase, all K_{u} mobile devices simultaneously transmit their data to the APs using the energy harvested from the previous downlink SWIPT phase. Based on Eq. (10), we can derive the uplink transmit power, denoted by $\mathcal{P}_m$, from mobile device m to the APs as follows:

$$\mathcal{P}_m = \frac{E_{\mathrm{r},m}}{n_{\mathrm{u}} T_s}. \tag{54}$$

We can derive the received signal, denoted by $\boldsymbol{Y}_{\mathrm{u},k}^{n_{\mathrm{u}}}$, from all mobile devices to AP k as follows:

$$\boldsymbol{Y}_{\mathrm{u},k}^{n_{\mathrm{u}}} = \sum_{m=1}^{K_{\mathrm{u}}} \sqrt{\eta_{\mathrm{u},m} \mathcal{P}_m} \boldsymbol{h}_{k,m} \boldsymbol{q}_m^{n_{\mathrm{u}}} + \boldsymbol{W}_{\mathrm{u},k}^{n_{\mathrm{u}}} \tag{55}$$

where $\eta_{\mathrm{u},m}$ is the uplink power allocation coefficient for mobile device m, $\boldsymbol{W}_{\mathrm{u},k}^{n_{\mathrm{u}}} \in \mathbb{C}^{N_{\mathrm{T}} \times n_{\mathrm{u}}}$ is the AWGN matrix with zero mean and covariance $\mathbf{I}_{N_{\mathrm{T}}}$ at AP k, and $\boldsymbol{q}_m^{n_{\mathrm{u}}}$ is the signal transmitted by mobile device m, which need to satisfy the following constraint:

$$\mathbb{E}\left[\| \boldsymbol{q}_m^{n_{\mathrm{u}}} \|^2 \right] = 1. \tag{56}$$

Then, after the conjugate precoder at the AP, the processed uplink signal, denoted by $\boldsymbol{r}_{\mathrm{u},m}$, at the CPU from mobile device

m can be derived as follows:

$$\begin{aligned}\boldsymbol{r}_{\mathrm{u},m}&=\sum_{k=1}^{K_\mathrm{a}}\left(\widehat{\boldsymbol{h}}_{k,m}\right)^H\boldsymbol{Y}_k^{n_\mathrm{u}}\\&=\sum_{m'=1}^{K_\mathrm{u}}\sum_{k=1}^{K_\mathrm{a}}\sqrt{\eta_{\mathrm{u},m'}\mathcal{P}_{m'}}\left(\widehat{\boldsymbol{h}}_{k,m}\right)^H\boldsymbol{h}_{k,m'}\boldsymbol{q}_{m'}^{n_\mathrm{u}}+\sum_{k=1}^{K_\mathrm{a}}\left(\widehat{\boldsymbol{h}}_{k,m}\right)^H\boldsymbol{w}_{\mathrm{u},k}^{n_\mathrm{u}}.\end{aligned}\tag{57}$$

Correspondingly, we can derive the uplink SNR, denoted by $\gamma_{\mathrm{u},m}$, at AP k as follows:

$$\begin{aligned}\gamma_{\mathrm{u},m}=\eta_{\mathrm{u},m}\mathcal{P}_m&\left|\mathbb{E}\left[\sum_{k=1}^{K_\mathrm{a}}(\widehat{\boldsymbol{h}}_{k,m})^H\boldsymbol{h}_{k,m}\right]\right|^2\left\{\sum_{m'=1}^{K_\mathrm{u}}\eta_{\mathrm{u},m'}\mathcal{P}_{m'}\right.\\&\times\mathbb{E}\left[\left|\sum_{k=1}^{K_\mathrm{a}}(\widehat{\boldsymbol{h}}_{k,m'})^H\boldsymbol{h}_{k,m}\right|^2\right]-\left|\mathbb{E}\left[\sum_{k=1}^{K_\mathrm{a}}(\widehat{\boldsymbol{h}}_{k,m})^H\boldsymbol{h}_{k,m}\right]\right|^2\\&\left.\times\eta_{\mathrm{u},m}\mathcal{P}_m+\mathbb{E}\left[\left\|\sum_{k=1}^{K_\mathrm{a}}\widehat{\boldsymbol{h}}_{k,m}\right\|^2\right]\right\}^{-1}.\end{aligned}\tag{58}$$

B. Joint Uplink Resource Allocation Optimization for Statistical Delay and Error-Rate Bounded QoS Provisioning Using FBC

Define the uplink ϵ-effective capacity, denoted by $EC_{\mathrm{u},m}^{\epsilon,\text{TS-PS}}(\theta_m)$, under joint TS-PS protocol for mobile device m as follows:

$$\begin{aligned}EC_{\mathrm{u},m}^{\epsilon,\text{TS-PS}}(\theta_m)=&-\frac{1}{\theta_m}\log\left\{\mathbb{E}_{\gamma_{\mathrm{u},m}}\left[\epsilon_{\mathrm{u},m}+(1-\epsilon_{\mathrm{u},m})\right.\right.\\&\left.\left.\times e^{-\theta_m n_\mathrm{u}T_s R_{\mathrm{u},m}}\right]\right\}\end{aligned}\tag{59}$$

where $\epsilon_{\mathrm{u},m}$ is the uplink decoding error probability for mobile device m and $R_{\mathrm{u},m}$ is the uplink coding rate, which is given as follows:

$$R_{\mathrm{u},m}=C\left(\gamma_{\mathrm{u},m}\right)-\sqrt{\frac{V\left(\gamma_{\mathrm{u},m}\right)}{n_\mathrm{u}}}Q^{-1}(\epsilon_{\mathrm{u},m})\tag{60}$$

where $C(\gamma_{\mathrm{u},m})$ and $V(\gamma_{\mathrm{u},m})$ are the uplink channel capacity and channel dispersion, respectively. Considering the joint TS-PS protocol, we define the uplink ϵ-effective capacity-energy region, denoted by $\mathcal{C}_{\mathrm{EC}_{\mathrm{u},m}^{\epsilon,\text{TS-PS}}-\mathrm{E}_m^{\text{TS-PS}}}$, as follows:

$$\begin{aligned}\mathcal{C}_{\mathrm{EC}_{\mathrm{u},m}^{\epsilon,\text{TS-PS}}-\mathrm{E}_m^{\text{TS-PS}}}\triangleq\bigcup_{\substack{0\le\eta_{k,m}\le1,\forall k\\0\le\alpha\le1\\0\le\rho\le1}}&\left\{\left(EC_{\mathrm{u},m}^{\epsilon,\text{TS-PS}},E_m^{\text{TS-PS}}\right):\right.\\EC_{\mathrm{u},m}^{\epsilon,\text{TS-PS}}\le-\frac{1}{\theta_m}&\log\left\{\mathbb{E}_{\gamma_{\mathrm{u},m}}\left[\epsilon_{\mathrm{u},m}+(1-\epsilon_{\mathrm{u},m})\,e^{-\theta_m n_\mathrm{u}T_s R_{\mathrm{u},m}}\right]\right\},\\E_m\le\alpha n_\mathrm{d}T_s\mathcal{P}_\mathrm{d}\zeta&\left|\sum_{k=1}^{K_\mathrm{a}}\sum_{m'=1}^{K_\mathrm{u}}\sqrt{\eta_{k,m'}}\left(\widehat{\boldsymbol{h}}_{k,m'}\right)^H\boldsymbol{h}_{k,m}\right|\\&+(1-\alpha)n_\mathrm{d}T_s\mathcal{P}_\mathrm{d}\rho\zeta\left|\sum_{k=1}^{K_\mathrm{a}}\sum_{m'=1}^{K_\mathrm{u}}\sqrt{\eta_{k,m'}}\left(\widehat{\boldsymbol{h}}_{k,m'}\right)^H\boldsymbol{h}_{k,m}\right|\left.\right\}.\end{aligned}\tag{61}$$

The max-min power control optimization is a centralized algorithm for guaranteeing a uniform SINR for all mobile devices. However, if an mobile device suffers from a bad channel gain and experiences poor SINR, the ϵ-effective capacity for all the other mobile devices will be compromised. Therefore, taking into account both the downlink harvested energy and uplink transmit power constraints, we formulate a distributed joint uplink resource allocation optimization problem for our proposed SWIPT-enabled CF m-MIMO based schemes under a joint TS-PS protocol in the finite blocklength regime as follows:

$$\mathbf{P_5}:\arg\max_{\substack{\alpha,\rho,n_\mathrm{d},n_\mathrm{u},\\\eta_{k,m},\eta_{\mathrm{u},m},\forall m,k}}\left\{\sum_{m=1}^{K_u}EC_{\mathrm{u},m}^{\epsilon,\text{TS-PS}}(\theta_m)\right\}\tag{62}$$

$$\text{s.t. } C1-C4;$$

$$C5:\gamma_{\mathrm{u},m}\ge\gamma_{\mathrm{th}},\quad\forall m;\tag{63}$$

$$C6:0\le\eta_{\mathrm{u},m}\le1,\quad\forall m,k,\tag{64}$$

where γ_{th} is the SNR threshold for all mobile devices. Then, the above optimization problem can be reformulated into the following equivalent minimization problem:

$$\mathbf{P_6}:\arg\min_{\substack{\alpha,\rho,n_\mathrm{d},n_\mathrm{u},\\\eta_{k,m},\eta_{\mathrm{u},m},\forall m,k}}\left\{\sum_{m=1}^{K_u}\mathbb{E}_{\gamma_{\mathrm{u},m}}\left[\epsilon_{\mathrm{u},m}+(1-\epsilon_{\mathrm{u},m})e^{-\theta_m n_\mathrm{u}T_s R_{\mathrm{u},m}}\right]\right\}\tag{65}$$

subject to the same constraints C1-C6 given by Eqs. (24)–(26), (46), (63), and (64), respectively. Since Theorem 1 and Theorem 2 have shown that $F(\gamma_{\mathrm{d},m})$ is convex in α, ρ, and n_d, $\eta_{k,m}$ respectively, we can easily obtain that the objective function in problem $\mathbf{P_6}$ is convex with respect to n_d and $\eta_{\mathrm{u},m}$, respectively, when the other parameters are fixed. Therefore, the optimization problem $\mathbf{P_6}$ specified by Eq. (65) is a convex optimization problem and thus can be efficiently solved by applying the SCA techniques with an iterative search method, which is similar to **Algorithm 1**.

V. Performance Evaluations

We use simulations to validate and evaluate our proposed SWIPT-enabled CF m-MIMO based schemes in the finite blocklength regime. Throughout our simulations, we set the number of APs $K_\mathrm{a}=100$, the number of mobile devices $K_\mathrm{u}=50$, the duration of each channel use $T_s=10\,\mu$s, the energy conversion efficiency $\zeta=0.5$, the uplink pilot transmit power $\mathcal{P}_\mathrm{p}=20$ dBm, and the downlink transmit power $\mathcal{P}_\mathrm{d}=80$ dBm.

We set the downlink blocklength error probability $\epsilon_{\mathrm{d},m}=1\times10^{-6}$. Using Eq. (66), Fig. 3 plots the second-order derivative $\partial^2F\left(\gamma_{\mathrm{d},m}\right)/\partial\alpha^2$ as a function of the downlink SNR $\gamma_{\mathrm{d},m}$ for our proposed SWIPT-enabled CF m-MIMO scheme using FBC. Fig. 3 shows that the second-order derivative $\partial^2F\left(\gamma_{\mathrm{d},m}\right)/\partial\alpha^2$ increases as the SNR $\gamma_{\mathrm{d},m}$ increases. In the high SNR region, we observe from Fig. 3 that $\partial^2F\left(\gamma_{\mathrm{d},m}\right)/\partial\alpha^2>0$, which implies

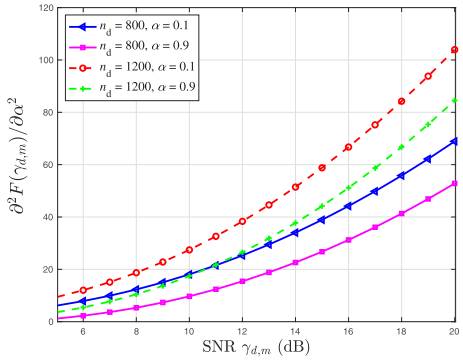

Fig. 3. The second-order derivative $\partial^2 F(\gamma_{\mathrm{d},m})/\partial\alpha^2$ vs. SNR $\gamma_{\mathrm{d},m}$ for our proposed SWIPT-enabled CF m-MIMO scheme using FBC with the TS factor $\alpha = 0.9$.

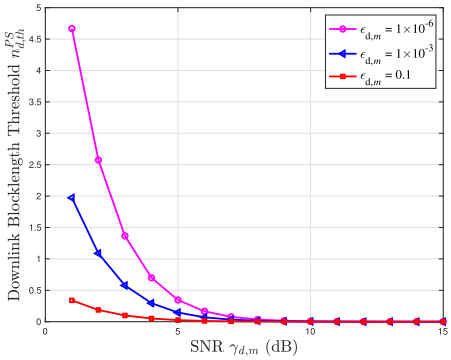

Fig. 5. The downlink blocklength threshold $n_{\mathrm{d,th}}^{\mathrm{PS}}$ vs. SNR $\gamma_{\mathrm{d},m}$ for our proposed SWIPT-enabled CF m-MIMO scheme under PS protocol using FBC.

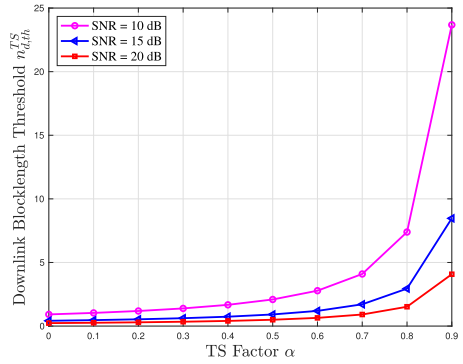

Fig. 4. The downlink blocklength threshold $n_{\mathrm{d,th}}^{\mathrm{TS}}$ vs. TS factor α for our proposed SWIPT-enabled CF m-MIMO scheme under TS protocol using FBC.

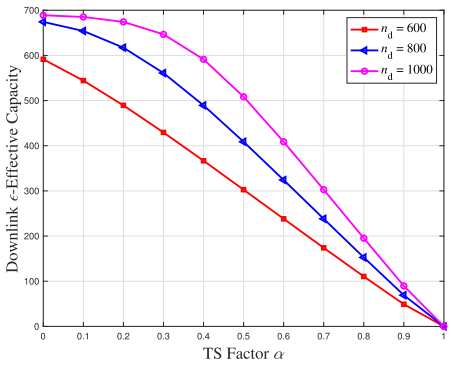

Fig. 6. The downlink ϵ-effective capacity vs. TS factor α for our proposed SWIPT-enabled CF m-MIMO scheme using FBC.

that the objective function in $\mathbf{P_2}$ specified by Eq. (27) is convex with respect to the TS factor α. Thus, Theorem 1 holds in the high SNR scenario. Fig. 3 also shows that $\partial^2 F(\gamma_{\mathrm{d},m})/\partial\alpha^2$ is an increasing function of the downlink blocklength n_{d}. This implies that a smaller value of n_{d} and a larger value of n_{d} set an lower bound and upper bound on the second-order derivative of the auxiliary function $\partial^2 F(\gamma_{\mathrm{d},m})/\partial\alpha^2$, respectively.

Using the downlink data blocklength threshold in Eq. (28), Fig. 4 depicts the threshold on downlink blocklength $n_{\mathrm{d,th}}^{\mathrm{TS}}$ as a function of TS factor α for our proposed SWIPT-enabled CF m-MIMO scheme under TS protocol in the finite blocklength regime. Fig. 4 shows that the threshold on downlink blocklength $n_{\mathrm{d,th}}^{\mathrm{TS}}$ increases as the TS factor α increases. Fig. 4 also shows that the threshold on downlink blocklength $n_{\mathrm{d,th}}^{\mathrm{TS}}$ is a decreasing function of SNR $\gamma_{\mathrm{d},m}$. We can observe from Fig. 4 that the value of $n_{\mathrm{d,th}}^{\mathrm{TS}}$ increases from 0.92 to 23.68 as the value of TS factor increases from 0 to 0.9 when the SNR is 10 dB. Since the authors in [16] have shown that the data transmission rate is quite accurate when the blocklength is as short as 100, the downlink blocklength threshold $n_{\mathrm{d,th}}^{\mathrm{TS}} \ll 100$ would automatically hold for $n > n_{\mathrm{d,th}}^{\mathrm{TS}}$, especially in the high SNR scenario, which validates Theorem 1.

In addition, using the downlink data blocklength threshold in Eq. (48), Fig. 5 plots the threshold on downlink blocklength $n_{\mathrm{d,th}}^{\mathrm{PS}}$ as a function of the SNR $\gamma_{\mathrm{d},m}$ for our proposed SWIPT-enabled CF m-MIMO scheme under PS protocol in the finite blocklength regime. Fig. 5 shows that the threshold on downlink blocklength $n_{\mathrm{d,th}}^{\mathrm{PS}}$ decreases as the SNR $\gamma_{\mathrm{d},m}$ increases. Fig. 5 also shows that the threshold on downlink blocklength $n_{\mathrm{d,th}}^{\mathrm{PS}}$ is a decreasing function of the decoding error probability $\epsilon_{\mathrm{d},m}$. We can observe from Fig. 5 that the value of $n_{\mathrm{d,th}}^{\mathrm{PS}}$ decreases from 4.67 to 0 as the value of SNR $\gamma_{\mathrm{d},m}$ increases from 0 to 15 dB when the decoding error probability $\epsilon_{\mathrm{d},m} = 1 \times 10^{-6}$. Since the data transmission rate is quite accurate when the blocklength is as short as 100 [16], the downlink blocklength threshold $n_{\mathrm{d,th}}^{\mathrm{PS}}$ would automatically hold for $n > n_{\mathrm{d,th}}^{\mathrm{PS}}$, which validates Theorem 2.

Setting the blocklength error probability $\epsilon_{\mathrm{d},m} = 1 \times 10^{-6}$, Fig. 6 plots the downlink ϵ-effective capacity as a function of TS factor α for our proposed SWIPT-enabled CF m-MIMO scheme using FBC. We can observe from Fig. 6 that the downlink ϵ-effective capacity is a decreasing function of TS factor α. In addition, Fig. 7 depicts the downlink ϵ-effective capacity as a function of both the TS factor α and QoS exponent θ_m for our proposed SWIPT-enabled CF m-MIMO scheme using FBC. We can observe from Fig. 7 that the downlink ϵ-effective capacity decreases as the decoding error probability $\epsilon_{\mathrm{d},m}$ increases. Fig. 7 also shows that the downlink ϵ-effective capacity is a decreasing function of QoS exponent θ_m, which implies that a smaller θ_m $(\theta_m \to 0)$ and a larger θ_m $(\theta_m \to \infty)$ lead to an upper

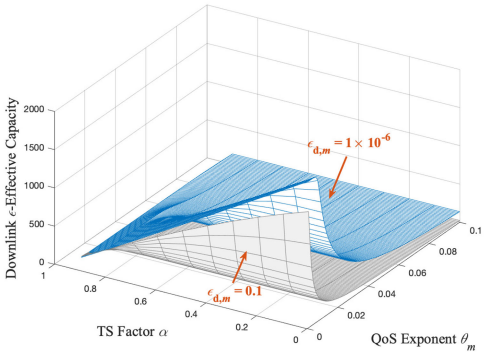

Fig. 7. The downlink ϵ-effective capacity vs. TS factor α and QoS exponent θ_m for our proposed SWIPT-enabled CF m-MIMO scheme using FBC.

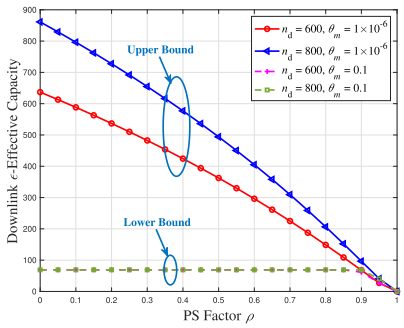

Fig. 8. The downlink ϵ-effective capacity vs. PS factor ρ for our proposed SWIPT-enabled CF m-MIMO scheme using FBC.

bound and lower bound on the downlink ϵ-effective capacity, respectively.

Setting the blocklength error probability $\epsilon_{\mathrm{d},m} = 1 \times 10^{-6}$, Fig. 8 plots the downlink ϵ-effective capacity as a function of PS factor ρ for our proposed SWIPT-enabled CF m-MIMO scheme in the finite blocklength regime. We can observe from Fig. 8 that the downlink ϵ-effective capacity is a decreasing function of PS factor ρ and is an increasing function of downlink data blocklength n_{d}. Fig. 8 also shows that the gap between the curves when $n_{\mathrm{d}} = 600$ and $n_{\mathrm{d}} = 800$ is negligible for large θ_m. This is because the downlink ϵ-effective capacity goes to zero when the delay-bounded QoS constraint is very stringent, i.e., $(\theta_m \to \infty)$.

Setting the downlink blocklength $n_{\mathrm{d}} = 1000$, downlink blocklength error probability $\epsilon_{\mathrm{d},m} = 1 \times 10^{-6}$, and uplink blocklength error probability $\epsilon_{\mathrm{u},m} = 1 \times 10^{-3}$, Fig. 9 depicts the uplink ϵ-effective capacity as a function of harvested energy for our proposed SWIPT-enabled CF m-MIMO scheme using FBC. Fig. 9 shows that the uplink ϵ-effective capacity is an increasing function of uplink data blocklength n_{u}. Fig. 9 shows that the uplink ϵ-effective capacity becomes negligible at the same operating point when $\alpha = 0$, $\rho = 0$, and $n_{\mathrm{u}} \in \{800, 1000, 1200\}$. This is due to the fact that when $\alpha = 0$ and $\rho = 0$, the entire downlink SWIPT phase are allocated for downlink information transfer, thus the mobile devices cannot harvest energy. On the other hand, when $\alpha, \rho \to 1$, the harvested energy becomes a maximum since the mobile devices perform energy harvesting for the entire downlink SWIPT phase. As a result, the uplink ϵ-effective capacity is an increasing function of the harvested energy.

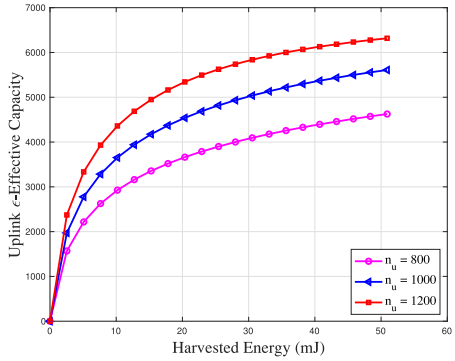

Fig. 9. The uplink ϵ-effective capacity vs. harvested energy for our proposed SWIPT-enabled CF m-MIMO scheme using FBC.

VI. Conclusions

We have proposed and developed statistical delay and error-rate bounded QoS provisioning schemes over SWIPT-enabled CF m-MIMO 6G wireless networks in the finite blocklength regime. In particular, we have developed SWIPT-enabled CF m-MIMO based system models using FBC. Taking into account both the harvested energy and transmit power constraints, we have formulated and solved the optimization problems for the tradeoff between the ϵ-effective capacity and harvested energy for both downlink SWIPT and uplink data transfer phases under statistical delay and error rate bounded QoS provisioning in supporting mURLLC. We have further conducted a set of simulations to validate and evaluate our proposed SWIPT-enabled CF m-MIMO schemes subject to statistical delay and error-rate bounded QoS constraints in the finite blocklength regime.

Appendix A
Table of Notations

The table for the summary of notations is listed in Table II on the next page.

Appendix B
Proof for $\partial^2 F(\gamma_{d,m})/\partial\alpha^2 > 0$ in Theorem 1

Plugging Eqs. (35) and (36) back into Eq. (34), we have

$$\frac{\partial^2 F(\gamma_{\mathrm{d},m})}{\partial \alpha^2} = \theta_m n_{\mathrm{d}} T_s \Bigg[-C(\gamma_{\mathrm{d},m}) + \sqrt{\frac{V(\gamma_{\mathrm{d},m})}{n_{\mathrm{d}}}} \frac{Q^{-1}(\epsilon_{\mathrm{d},m})}{2} \times (1-\alpha)^{-\frac{1}{2}} \Bigg]^2 - \sqrt{\frac{V(\gamma_{\mathrm{d},m})}{n_{\mathrm{d}}}} \frac{Q^{-1}(\epsilon_{\mathrm{d},m})(1-\alpha)^{-\frac{3}{2}}}{4}$$

$$= \theta_m n_{\mathrm{d}} T_s \Bigg\{ [C(\gamma_{\mathrm{d},m})]^2 + \frac{V(\gamma_{\mathrm{d},m}) \left[Q^{-1}(\epsilon_{\mathrm{d},m})\right]^2}{4 n_{\mathrm{d}} (1-\alpha)} - C(\gamma_{\mathrm{d},m}) \sqrt{\frac{V(\gamma_{\mathrm{d},m})}{n_{\mathrm{d}}}} Q^{-1}(\epsilon_{\mathrm{d},m})(1-\alpha)^{-\frac{1}{2}} \Bigg\}$$

TABLE II
SUMMARY OF NOTATION

K_a	Number of APs	K_u	Number of mobile users
N_{T}	Number of antennas at the AP	n_{p}	Number of channel uses for uplink pilot training
ρ	PS factor	n_{u}	Number of channel uses for uplink data transmission
α	TS factor	n_{d}	Number of channel uses for downlink SWIPT
$\beta_{k,m}$	Large-scale fading coefficient	$\boldsymbol{h}_{k,m}$	Channel's impulse response vector
$\boldsymbol{g}_{k,m}$	Small-scale Rayleigh fading vector	$\boldsymbol{\phi}_m^{n_{\mathrm{p}}}$	Pilot training sequence
$\boldsymbol{Y}_k^{n_{\mathrm{p}}}$	Received signal matrix	$\mathcal{P}_{\mathrm{p}}$	Uplink pilot transmit power
$\boldsymbol{W}_{\mathrm{p},k}$	AWGN matrix	$\mathbf{R}_{\mathbf{h}_{k,m}}$	Covariance matrix of $\mathbf{h}_{k,m}$
$\widehat{\boldsymbol{h}}_{k,m}$	MMSE estimator of $\mathbf{h}_{k,m}$	E_m^{TS}	Harvested energy at TS receiver
E_m^{PS}	Harvested energy at PS receiver	ζ	Energy conversion efficiency
T_s	Duration of each channel use	$\mathcal{P}_{\mathrm{d}}$	Power for downlink transmission
E_m	Total harvested energy	B_m	Charging state of battery
$E_{\mathrm{r},m}$	Remaining energy	$\boldsymbol{X}_k^{n_{\mathrm{d}}}$	Downlink transmit signal matrix
$\boldsymbol{y}_{\mathrm{d},m}^{n_{\mathrm{d}}}$	Downlink receive signal	$\epsilon_{\mathrm{d},m}$	Downlink decoding error probability
$\gamma_{\mathrm{d},m}$	SNR	$\eta_{k,m}$	Downlink power allocation coefficient
$\boldsymbol{b}_{k,m}$	Precoder vector	$R_{\mathrm{d},m}$	Maximum achievable downlink coding rate
$C\left(\gamma_{\mathrm{d},m}\right)$	Channel capacity	$V\left(\gamma_{\mathrm{d},m}\right)$	Channel dispersion
θ_m	QoS exponent	$\overline{E}_{\min}$	Minimum required harvested energy
Q_{th}	Queuing threshold	$EC_{\mathrm{d},m}^{\epsilon}(\theta_m)$	Downlink ϵ-effective capacity
$\boldsymbol{Y}_{\mathrm{u},k}^{n_{\mathrm{u}}}$	Uplink received signal	$\eta_{\mathrm{u},m}$	Uplink power allocation coefficient
$\boldsymbol{W}_{\mathrm{u},k}^{n_{\mathrm{u}}}$	Uplink AWGN matrix	$\epsilon_{\mathrm{u},m}$	Uplink decoding error probability
$\gamma_{\mathrm{u},m}$	Uplink SNR	$EC_{\mathrm{u},m}^{\epsilon,\text{TS-PS}}(\theta_m)$	ϵ-effective capacity under joint TS-PS protocol
$R_{\mathrm{u},m}$	Uplink coding rate	$C\left(\gamma_{\mathrm{u},m}\right)$	Uplink channel capacity
$V\left(\gamma_{\mathrm{u},m}\right)$	Uplink channel dispersion	$\mathcal{C}_{\mathrm{EC}_{\mathrm{u},m}^{\epsilon,\text{TS-PS}}-\mathrm{E}_m^{\text{TS-PS}}}$	Uplink ϵ-effective capacity-energy region

$$
\begin{aligned}
&- \sqrt{\frac{V\left(\gamma_{\mathrm{d},m}\right)}{n_{\mathrm{d}}}} \frac{Q^{-1}(\epsilon_{\mathrm{d},m})\left(1-\alpha\right)^{-\frac{3}{2}}}{4} \\
&> \theta_m n_{\mathrm{d}} T_s \Bigg\{ \left[C\left(\gamma_{\mathrm{d},m}\right)\right]^2 - C\left(\gamma_{\mathrm{d},m}\right) \sqrt{\frac{V\left(\gamma_{\mathrm{d},m}\right)}{n_{\mathrm{d}}}} Q^{-1}(\epsilon_{\mathrm{d},m}) \\
&\times \left(1-\alpha\right)^{-\frac{1}{2}} \Bigg\} - \sqrt{\frac{V\left(\gamma_{\mathrm{d},m}\right)}{n_{\mathrm{d}}}} \frac{Q^{-1}(\epsilon_{\mathrm{d},m})\left(1-\alpha\right)^{-\frac{3}{2}}}{4}.
\end{aligned} \tag{66}
$$

Using Eq. (18), we get

$$
\sqrt{\frac{V\left(\gamma_{\mathrm{d},m}\right)}{(1-\alpha)n_{\mathrm{d}}}} Q^{-1}(\epsilon_{\mathrm{d},m}) = C\left(\gamma_{\mathrm{d},m}\right) - R_{\mathrm{d},m}. \tag{67}
$$

Thus, plugging Eq. (67) back into Eq. (66), we can obtain the following equation:

$$
\begin{aligned}
\frac{\partial^2 F\left(\gamma_{\mathrm{d},m}\right)}{\partial \alpha^2} &> \theta_m n_{\mathrm{d}} T_s \Bigg\{ \left[C\left(\gamma_{\mathrm{d},m}\right)\right]^2 - C\left(\gamma_{\mathrm{d},m}\right) \Big[C\left(\gamma_{\mathrm{d},m}\right) \\
&\quad - R_{\mathrm{d},m} \Big] \Bigg\} - \frac{C\left(\gamma_{\mathrm{d},m}\right) - R_{\mathrm{d},m}}{4(1-\alpha)} \\
&= \theta_m n_{\mathrm{d}} T_s C\left(\gamma_{\mathrm{d},m}\right) R_{\mathrm{d},m} - \frac{C\left(\gamma_{\mathrm{d},m}\right) - R_{\mathrm{d},m}}{4(1-\alpha)} \\
&= \frac{1}{R_{\mathrm{d},m}} \Bigg[\theta_m n_{\mathrm{d}} T_s C\left(\gamma_{\mathrm{d},m}\right) + \frac{1}{4(1-\alpha)} \\
&\quad - \frac{C\left(\gamma_{\mathrm{d},m}\right)}{4(1-\alpha) R_{\mathrm{d},m}} \Bigg]
\end{aligned} \tag{68}
$$

Based on Eq. (18), we can obtain that

$$
\frac{C\left(\gamma_{\mathrm{d},m}\right)}{R_{\mathrm{d},m}} < \frac{C\left(\gamma_{\mathrm{d},m}\right)}{C\left(\gamma_{\mathrm{d},m}\right) - \sqrt{\frac{1}{(1-\alpha)n_{\mathrm{d}}}} Q^{-1}(\epsilon_{\mathrm{d},m})}. \tag{69}
$$

Thus, plugging Eq. (69) back into Eq. (68), we have

$$
\begin{aligned}
\frac{\partial^2 F\left(\gamma_{\mathrm{d},m}\right)}{\partial \alpha^2} &> \frac{4(1-\alpha)}{R_{\mathrm{d},m}} \Bigg\{ 4(1-\alpha)\theta_m n_{\mathrm{d}} T_s C\left(\gamma_{\mathrm{d},m}\right) + 1 \\
&\quad - \frac{C\left(\gamma_{\mathrm{d},m}\right)}{C\left(\gamma_{\mathrm{d},m}\right) - \sqrt{\frac{1}{(1-\alpha)n_{\mathrm{d}}}} Q^{-1}(\epsilon_{\mathrm{d},m})} \Bigg\} \\
&= \frac{4(1-\alpha)}{R_{\mathrm{d},m}} \Bigg\{ \frac{C\left(\gamma_{\mathrm{d},m}\right)}{C\left(\gamma_{\mathrm{d},m}\right) - \sqrt{\frac{1}{(1-\alpha)n_{\mathrm{d,th}}^{\mathrm{TS}}}} Q^{-1}(\epsilon_{\mathrm{d},m})} \\
&\quad - \frac{C\left(\gamma_{\mathrm{d},m}\right)}{C\left(\gamma_{\mathrm{d},m}\right) - \sqrt{\frac{1}{(1-\alpha)n_{\mathrm{d}}}} Q^{-1}(\epsilon_{\mathrm{d},m})} \Bigg\}
\end{aligned} \tag{70}
$$

where $n_{\mathrm{d,th}}^{\mathrm{TS}}$ is given by Eq. (28). Applying the condition: $n_{\mathrm{d}} > n_{\mathrm{d,th}}^{\mathrm{TS}}$ into Eq. (70), which implies that $\left[(1-\alpha)n_{\mathrm{d,th}}^{\mathrm{TS}}\right]^{-\frac{1}{2}} > \left[(1-\alpha)n_{\mathrm{d}}\right]^{-\frac{1}{2}}$, and thus we can obtain the following equation:

$$
\frac{\partial^2 F\left(\gamma_{\mathrm{d},m}\right)}{\partial \alpha^2} > 0. \tag{71}
$$

APPENDIX C
PROOF FOR $\partial^2 R_{d,m}/\partial \rho^2 < 0$ IN THEOREM 2

To determine whether $\partial^2 R_{\mathrm{d},m}/\partial \rho^2 < 0$, first we obtain the second-order derivatives of the downlink channel capacity $C(\gamma_{\mathrm{d},m})$ and channel dispersion $V(\gamma_{\mathrm{d},m})$ with respect to the

PS factor ρ, respectively, as follows:

$$\frac{\partial^2 C\left(\gamma_{\mathrm{d},m}\right)}{\partial \rho^2} = -\frac{1}{\left(\log 2\right)\left(1+\gamma_{\mathrm{d},m}\right)^2}\left(\frac{\partial \gamma_{\mathrm{d},m}}{\partial \rho}\right)^2 + \frac{\partial^2 \gamma_{\mathrm{d},m}}{\partial \rho^2} \times \frac{1}{\left(\log 2\right)\left(1+\gamma_{\mathrm{d},m}\right)} \tag{72}$$

and

$$\frac{\partial^2 V\left(\gamma_{\mathrm{d},m}\right)}{\partial \rho^2} = -6\left(1+\gamma_{\mathrm{d},m}\right)^{-4}\left(\frac{\partial \gamma_{\mathrm{d},m}}{\partial \rho}\right)^2 + 2\left(1+\gamma_{\mathrm{d},m}\right)^{-3} \times \frac{\partial^2 \gamma_{\mathrm{d},m}}{\partial \rho^2}. \tag{73}$$

Then, using Eqs. (72) and (73), we obtain the second-order derivative of $R_{\mathrm{d},m}$ with respect to the PS factor ρ as follows:

$$\begin{aligned}
\frac{\partial^2 R_{\mathrm{d},m}}{\partial \rho^2} &= \frac{\partial^2 C\left(\gamma_{\mathrm{d},m}\right)}{\partial \rho^2} + \frac{Q^{-1}(\epsilon_{\mathrm{d},m})}{4\sqrt{n_{\mathrm{d}}}}\left[V\left(\gamma_{\mathrm{d},m}\right)\right]^{-\frac{3}{2}} \\
&\quad \times \left[\frac{\partial V\left(\gamma_{\mathrm{d},m}\right)}{\partial \rho}\right]^2 - \frac{Q^{-1}(\epsilon_{\mathrm{d},m})}{2\sqrt{n_{\mathrm{d}}}}\left[V\left(\gamma_{\mathrm{d},m}\right)\right]^{-\frac{1}{2}}\frac{\partial^2 V\left(\gamma_{\mathrm{d},m}\right)}{\partial \rho^2} \\
&= -\frac{1}{\left(\log 2\right)\left(1+\gamma_{\mathrm{d},m}\right)^2}\left(\frac{\partial \gamma_{\mathrm{d},m}}{\partial \rho}\right)^2 + \frac{1}{\left(\log 2\right)\left(1+\gamma_{\mathrm{d},m}\right)} \\
&\quad \times \frac{\partial^2 \gamma_{\mathrm{d},m}}{\partial \rho^2} + \frac{Q^{-1}(\epsilon_{\mathrm{d},m})}{4\sqrt{n_{\mathrm{d}}}}\left[V\left(\gamma_{\mathrm{d},m}\right)\right]^{-\frac{3}{2}}\Bigg[-6\left(1+\gamma_{\mathrm{d},m}\right)^{-4} \\
&\quad \times \left(\frac{\partial \gamma_{\mathrm{d},m}}{\partial \rho}\right)^2 + 2\left(1+\gamma_{\mathrm{d},m}\right)^{-3}\frac{\partial^2 \gamma_{\mathrm{d},m}}{\partial \rho^2}\Bigg]^2 - \frac{Q^{-1}(\epsilon_{\mathrm{d},m})}{2\sqrt{n_{\mathrm{d}}}} \\
&\quad \times \left[V\left(\gamma_{\mathrm{d},m}\right)\right]^{-\frac{1}{2}}\Bigg[-6\left(1+\gamma_{\mathrm{d},m}\right)^{-4}\left(\frac{\partial \gamma_{\mathrm{d},m}}{\partial \rho}\right)^2 + \frac{\partial^2 \gamma_{\mathrm{d},m}}{\partial \rho^2} \\
&\quad \times 2\left(1+\gamma_{\mathrm{d},m}\right)^{-3}\Bigg] \\
&= -\frac{1}{\left(\log 2\right)\left(1+\gamma_{\mathrm{d},m}\right)^2}\left(\frac{\partial \gamma_{\mathrm{d},m}}{\partial \rho}\right)^2 + \frac{1}{\left(\log 2\right)\left(1+\gamma_{\mathrm{d},m}\right)} \\
&\quad \times \frac{\partial^2 \gamma_{\mathrm{d},m}}{\partial \rho^2} - \frac{Q^{-1}(\epsilon_{\mathrm{d},m})}{2\sqrt{n_{\mathrm{d}}}}\left[V\left(\gamma_{\mathrm{d},m}\right)\right]^{-\frac{1}{2}}\Bigg[-6\left(1+\gamma_{\mathrm{d},m}\right)^{-4} \\
&\quad \times \left(\frac{\partial \gamma_{\mathrm{d},m}}{\partial \rho}\right)^2 + 2\left(1+\gamma_{\mathrm{d},m}\right)^{-3}\frac{\partial^2 \gamma_{\mathrm{d},m}}{\partial \rho^2}\Bigg]\Bigg\{1 - \frac{1}{2V\left(\gamma_{\mathrm{d},m}\right)} \\
&\quad \times \left[-6\left(1+\gamma_{\mathrm{d},m}\right)^{-4}\left(\frac{\partial \gamma_{\mathrm{d},m}}{\partial \rho}\right)^2 + 2\left(1+\gamma_{\mathrm{d},m}\right)^{-3}\frac{\partial^2 \gamma_{\mathrm{d},m}}{\partial \rho^2}\right]\Bigg\}.
\end{aligned} \tag{74}$$

Second, we can rewrite the SNR function given by Eq. (16) as follows:

$$\gamma_{\mathrm{d},m} = \frac{(1-\rho)\gamma_{1,m}}{(1-\rho)\gamma_{2,m}+1} \tag{75}$$

where

$$\begin{cases}
\gamma_{1,m} = \mathcal{P}_{\mathrm{d}}\left|\mathbb{E}\left[\sum\limits_{k=1}^{K_{\mathrm{a}}}\sqrt{\eta_{k,m}}(\boldsymbol{h}_{k,m})^H\boldsymbol{b}_{k,m}\right]\right|^2; \\
\gamma_{2,m} = \mathcal{P}_{\mathrm{d}}\sum\limits_{m'=1}^{K_{\mathrm{u}}}\mathbb{E}\left[\left|\sum_{k=1}^{K_{\mathrm{a}}}\sqrt{\eta_{k,m'}}(\boldsymbol{h}_{k,m'})^H\boldsymbol{b}_{k,m}\right|^2\right] \\
\qquad -\mathcal{P}_{\mathrm{d}}\left|\mathbb{E}\left[\sum\limits_{k=1}^{K_{\mathrm{a}}}\sqrt{\eta_{k,m}}(\boldsymbol{h}_{k,m})^H\boldsymbol{b}_{k,m}\right]\right|^2.
\end{cases} \tag{76}$$

Using Eq. (16), we characterize the first-order and second-order derivatives of $\gamma_{\mathrm{d},m}$ with respect to the PS factor ρ as follows:

$$\begin{cases}
\frac{\partial \gamma_{\mathrm{d},m}}{\partial \rho} = \frac{-\gamma_{1,m}}{[(1-\rho)\gamma_{2,m}+1]^2}; \\
\frac{\partial^2 \gamma_{\mathrm{d},m}}{\partial \rho^2} = \frac{-2\gamma_{1,m}\gamma_{2,m}}{[(1-\rho)\gamma_{2,m}+1]^3}.
\end{cases} \tag{77}$$

Plugging Eq. (77) back into Eq. (74), we can obtain:

$$\begin{aligned}
\frac{\partial^2 R_{\mathrm{d},m}}{\partial \rho^2} &< -\frac{1}{\left(\log 2\right)\left(1+\gamma_{\mathrm{d},m}\right)^2}\left(\frac{\partial \gamma_{\mathrm{d},m}}{\partial \rho}\right)^2 + \frac{1}{\left(\log 2\right)\left(1+\gamma_{\mathrm{d},m}\right)} \\
&\quad \times \frac{\partial^2 \gamma_{\mathrm{d},m}}{\partial \rho^2} - \frac{Q^{-1}(\epsilon_{\mathrm{d},m})}{2\sqrt{n_{\mathrm{d}}}}\left[V\left(\gamma_{\mathrm{d},m}\right)\right]^{-\frac{1}{2}}\Bigg[-6\left(1+\gamma_{\mathrm{d},m}\right)^{-4} \\
&\quad \times \left(\frac{\partial \gamma_{\mathrm{d},m}}{\partial \rho}\right)^2 + 2\left(1+\gamma_{\mathrm{d},m}\right)^{-3}\frac{\partial^2 \gamma_{\mathrm{d},m}}{\partial \rho^2}\Bigg].
\end{aligned} \tag{78}$$

Then, in order to guarantee $\partial^2 R_{\mathrm{d},m}/\partial \rho^2 < 0$, it is sufficient to have

$$\begin{aligned}
&-\frac{1}{\left(\log 2\right)\left(1+\gamma_{\mathrm{d},m}\right)^2}\left(\frac{\partial \gamma_{\mathrm{d},m}}{\partial \rho}\right)^2 + \frac{1}{\left(\log 2\right)\left(1+\gamma_{\mathrm{d},m}\right)}\frac{\partial^2 \gamma_{\mathrm{d},m}}{\partial \rho^2} \\
&< \frac{Q^{-1}(\epsilon_{\mathrm{d},m})}{2\sqrt{n_{\mathrm{d}}}}\left[V\left(\gamma_{\mathrm{d},m}\right)\right]^{-\frac{1}{2}}\Bigg[-6\left(1+\gamma_{\mathrm{d},m}\right)^{-4}\left(\frac{\partial \gamma_{\mathrm{d},m}}{\partial \rho}\right)^2 \\
&\qquad + 2\left(1+\gamma_{\mathrm{d},m}\right)^{-3}\frac{\partial^2 \gamma_{\mathrm{d},m}}{\partial \rho^2}\Bigg]
\end{aligned} \tag{79}$$

which leads to the following inequality:

$$\begin{aligned}
&\frac{1}{(\log 2)(1+\gamma_{\mathrm{d},m})}\frac{\partial^2 \gamma_{\mathrm{d},m}}{\partial \rho^2} - \frac{Q^{-1}(\epsilon_{\mathrm{d},m})}{\sqrt{n_{\mathrm{d}}V(\gamma_{\mathrm{d},m})}}(1+\gamma_{\mathrm{d},m})^{-3}\frac{\partial^2 \gamma_{\mathrm{d},m}}{\partial \rho^2} \\
&< \frac{1}{\left(\log 2\right)\left(1+\gamma_{\mathrm{d},m}\right)^2}\left(\frac{\partial \gamma_{\mathrm{d},m}}{\partial \rho}\right)^2 - \frac{3Q^{-1}(\epsilon_{\mathrm{d},m})}{\sqrt{n_{\mathrm{d}}V\left(\gamma_{\mathrm{d},m}\right)}} \\
&\quad \times \left(1+\gamma_{\mathrm{d},m}\right)^{-4}\left(\frac{\partial \gamma_{\mathrm{d},m}}{\partial \rho}\right)^2
\end{aligned} \tag{80}$$

Then, we get

$$\begin{aligned}
&\left[\frac{1}{\left(\log 2\right)\left(1+\gamma_{\mathrm{d},m}\right)} - \frac{Q^{-1}(\epsilon_{\mathrm{d},m})}{\sqrt{n_{\mathrm{d}}V\left(\gamma_{\mathrm{d},m}\right)}}\left(1+\gamma_{\mathrm{d},m}\right)^{-3}\right]\frac{\partial^2 \gamma_{\mathrm{d},m}}{\partial \rho^2} \\
&< \left[\frac{1}{(\log 2)(1+\gamma_{\mathrm{d},m})^2} - \frac{3Q^{-1}(\epsilon_{\mathrm{d},m})}{\sqrt{n_{\mathrm{d}}V(\gamma_{\mathrm{d},m})}}(1+\gamma_{\mathrm{d},m})^{-4}\right]\left(\frac{\partial \gamma_{\mathrm{d},m}}{\partial \rho}\right)^2.
\end{aligned} \tag{81}$$

Since $\partial^2 \gamma_{\mathrm{d},m}/\partial \rho^2 < 0$ and $Q^{-1}(\epsilon_{\mathrm{d},m})$ when $\epsilon_{\mathrm{d},m} \in (0, 0.5)$, to guarantee Eq. (81) holds, it is equivalent to show that the

following inequalities hold:

$$\begin{cases} \frac{1}{(\log 2)(1+\gamma_{\mathrm{d},m})} - \frac{Q^{-1}(\epsilon_{\mathrm{d},m})}{\sqrt{n_{\mathrm{d}}V(\gamma_{\mathrm{d},m})}}\left(1+\gamma_{\mathrm{d},m}\right)^{-3} > 0; \\ \frac{1}{(\log 2)(1+\gamma_{\mathrm{d},m})^2} - \frac{3Q^{-1}(\epsilon_{\mathrm{d},m})}{\sqrt{n_{\mathrm{d}}V(\gamma_{\mathrm{d},m})}}\left(1+\gamma_{\mathrm{d},m}\right)^{-4} > 0, \end{cases} \tag{82}$$

which leads to the following inequalities:

$$\begin{cases} \sqrt{n_{\mathrm{d}}V\left(\gamma_{\mathrm{d},m}\right)} > \frac{Q^{-1}(\epsilon_{\mathrm{d},m})(\log 2)}{\left(1+\gamma_{\mathrm{d},m}\right)^2}; \\ \sqrt{n_{\mathrm{d}}V\left(\gamma_{\mathrm{d},m}\right)} > \frac{3Q^{-1}(\epsilon_{\mathrm{d},m})(\log 2)}{\left(1+\gamma_{\mathrm{d},m}\right)^2}. \end{cases} \tag{83}$$

Thus, using Eq. (83), we can obtain the lower bound on the downlink data blocklength to guarantee $\partial^2 R_{\mathrm{d},m}/\partial\rho^2 < 0$ as follows:

$$n_{\mathrm{d}} > \frac{9}{V\left(\gamma_{\mathrm{d},m}\right)}\left[\frac{Q^{-1}(\epsilon_{\mathrm{d},m})(\log 2)}{\left(1+\gamma_{\mathrm{d},m}\right)^2}\right]^2. \tag{84}$$

Finally, we can obtain $\partial^2 R_{\mathrm{d},m}/\partial\rho^2 < 0$.

REFERENCES

[1] H. Ji, S. Park, J. Yeo, Y. Kim, J. Lee, and B. Shim, "Ultra-reliable and low-latency communications in 5G downlink: Physical layer aspects," *IEEE Wireless Commun.*, vol. 25, no. 3, pp. 124–130, Jun. 2018.

[2] W. Saad, M. Bennis, and M. Chen, "A vision of 6G wireless systems: Applications, trends, technologies, and open research problems," *IEEE Netw.*, vol. 34, no. 3, pp. 134–142, May/Jun. 2020.

[3] K. Banawan and S. Ulukus, "MIMO wiretap channel under receiver-side power constraints with applications to wireless power transfer and cognitive radio," *IEEE Trans. Commun.*, vol. 64, no. 9, pp. 3872–3885, Sep. 2016.

[4] X. Zhang, J. Tang, H.-H. Chen, S. Ci, and M. Guizani, "Cross-layer-based modeling for quality of service guarantees in mobile wireless networks," *IEEE Commun. Mag.*, vol. 44, no. 1, pp. 100–106, Jan. 2006.

[5] J. Tang and X. Zhang, "Quality-of-service driven power and rate adaptation over wireless links," *IEEE Trans. Wireless Commun.*, vol. 6, no. 8, pp. 3058–3068, Dec. 2007.

[6] J. Tang and X. Zhang, "Cross-layer resource allocation over wireless relay networks for quality of service provisioning," *IEEE J. Sel. Areas Commun.*, vol. 25, no. 4, pp. 645–656, May 2007.

[7] X. Zhang and J. Tang, "Power-delay tradeoff over wireless networks," *IEEE Trans. Commun.*, vol. 61, no. 9, pp. 3673–3684, Sep. 2013.

[8] J. Tang and X. Zhang, "Cross-layer modeling for quality of service guarantees over wireless links," *IEEE Trans. Wireless Commun.*, vol. 6, no. 12, pp. 4504–4512, Dec. 2007.

[9] J. Tang and X. Zhang, "Quality-of-service driven power and rate adaptation for multichannel communications over wireless links," *IEEE Trans. Wireless Commun.*, vol. 6, no. 12, pp. 4349–4360, Dec. 2007.

[10] J. Tang and X. Zhang, "Cross-layer-model based adaptive resource allocation for statistical QoS guarantees in mobile wireless networks," *IEEE Trans. Wireless Commun.*, vol. 7, no. 6, pp. 2318–2328, Jun. 2008.

[11] X. Zhang and Q. Du, "Adaptive low-complexity erasure-correcting code-based protocols for QoS-driven mobile multicast services over wireless networks," *IEEE Trans. Veh. Technol.*, vol. 55, no. 5, pp. 1633–1647, Sep. 2006.

[12] Q. Du and X. Zhang, "Statistical QoS provisionings for wireless unicast/multicast of multi-layer video streams," *IEEE J. Sel. Areas Commun.*, vol. 28, no. 3, pp. 420–433, Apr. 2010.

[13] Q. Du and X. Zhang, "QoS-aware base-station selections for distributed MIMO links in broadband wireless networks," *IEEE J. Sel. Areas Commun.*, vol. 29, no. 6, pp. 1123–1138, Jun. 2011.

[14] H. Su and X. Zhang, "Cross-layer based opportunistic MAC protocols for QoS provisionings over cognitive radio wireless networks," *IEEE J. Sel. Areas Commun.*, vol. 26, no. 1, pp. 118–129, Jan. 2008.

[15] Y. Polyanskiy, H. V. Poor, and S. Verdú, "Feedback in the non-asymptotic regime," *IEEE Trans. Inf. Theory*, vol. 57, no. 8, pp. 4903–4925, Aug. 2011.

[16] Y. Polyanskiy, H. V. Poor, and S. Verdú, "Channel coding rate in the finite blocklength regime," *IEEE Trans. Inf. Theory*, vol. 56, no. 5, pp. 2307–2359, May 2010.

[17] P. Mary, J. Gorce, A. Unsal, and H. V. Poor, "Finite blocklength information theory: What is the practical impact on wireless communications?" in *Proc. IEEE Globecom Workshops*, 2016, pp. 1–6.

[18] W. Yang, G. Durisi, T. Koch, and Y. Polyanskiy, "Quasi-static multiple-antenna fading channels at finite blocklength," *IEEE Trans. Inf. Theory*, vol. 60, no. 7, pp. 4232–4265, Jul. 2014.

[19] B. Makki, T. Svensson, M. Coldrey, and M.-S. Alouini, "Finite block-length analysis of large-but-finite MIMO systems," *IEEE Wireless Commun. Lett.*, vol. 8, no. 1, pp. 113–116, Feb. 2019.

[20] M. Varasteh, B. Rassouli, and B. Clerckx, "On capacity-achieving distributions for complex AWGN channels under nonlinear power constraints and their applications to SWIPT," *IEEE Trans. Inf. Theory*, vol. 66, no. 10, pp. 6488–6508, Oct. 2020.

[21] Z. Wang, H. Zhao, S. Wang, J. Zhang, and M. Alouini, "Secrecy analysis in SWIPT systems over generalized-k fading channels," *IEEE Commun. Lett.*, vol. 23, no. 5, pp. 834–837, May 2019.

[22] G. Amarasuriya, E. G. Larsson, and H. V. Poor, "Wireless information and power transfer in multiway massive MIMO relay networks," *IEEE Trans. Wireless Commun.*, vol. 15, no. 6, pp. 3837–3855, Jun. 2016.

[23] T. D. P. Perera, D. N. K. Jayakody, S. K. Sharma, S. Chatzinotas, and J. Li, "Simultaneous wireless information and power transfer (SWIPT): Recent advances and future challenges," *IEEE Commun. Surv. Tut.*, vol. 20, no. 1, pp. 264–302, Jan.–Mar. 2018.

[24] L. R. Varshney, "Transporting information and energy simultaneously," in *Proc. IEEE Int. Symp. Inf. Theory*, 2008, pp. 1612–1616.

[25] O. L. A. López, E. M. G. Fernández, R. D. Souza, and H. Alves, "Ultra-reliable cooperative short-packet communications with wireless energy transfer," *IEEE Sensors J.*, vol. 18, no. 5, pp. 2161–2177, Mar. 2018.

[26] A. Agarwal, A. K. Jagannatham, and L. Hanzo, "Finite blocklength non-orthogonal cooperative communication relying on SWIPT-enabled energy harvesting relays," *IEEE Trans. Commun.*, vol. 68, no. 6, pp. 3326–3341, Jun. 2020.

[27] O. L. A. López, E. M. G. Fernández, R. D. Souza, and H. Alves, "Wireless powered communications with finite battery and finite blocklength," *IEEE Trans. Commun.*, vol. 66, no. 4, pp. 1803–1816, Apr. 2018.

[28] S. M. Perlaza, A. Tajer, and H. V. Poor, "Simultaneous information and energy transmission: A finite block-length analysis," in *Proc. IEEE 19th Int. Workshop Signal Process. Adv. Wireless Commun.*, 2018, pp. 1–5.

[29] I. Kim, D. I. Kim, and J. Kang, "Rate-energy tradeoff and decoding error probability-energy tradeoff for SWIPT in finite code length," *IEEE Trans. Wireless Commun.*, vol. 16, no. 12, pp. 8220–8234, Dec. 2017.

[30] X. Zhang, J. Wang, and H. V. Poor, "Statistical delay and error-rate bounded QoS provisioning for mURLLC over 6G CF M-MIMO mobile networks in the finite blocklength regime," *IEEE J. Sel. Areas Commun.*, vol. 39, no. 3, pp. 652–667, Mar. 2021.

[31] H. Q. Ngo, A. Ashikhmin, H. Yang, E. G. Larsson, and T. L. Marzetta, "Cell-free massive MIMO versus small cells," *IEEE Trans. Wireless Commun.*, vol. 16, no. 3, pp. 1834–1850, Mar. 2017.

[32] M. Alonzo, S. Buzzi, A. Zappone, and C. D'Elia, "Energy-efficient power control in cell-free and user-centric massive MIMO at millimeter wave," *IEEE Trans. Green Commun. Netw.*, vol. 3, no. 3, pp. 651–663, Sep. 2019.

[33] S. Kusaladharma, W. P. Zhu, W. Ajib, and G. A. A. Baduge, "Stochastic geometry based performance characterization of SWIPT in cell-free massive MIMO," *IEEE Trans. Veh. Technol.*, vol. 69, no. 11, pp. 13357–13370, Nov. 2020.

[34] R. Shrestha and G. Amarasuriya, "SWIPT in cell-free massive MIMO," in *Proc. IEEE Global Commun. Conf.*, 2018, pp. 1–7.

[35] M. Alageli, A. Ikhlef, F. Alsifiany, M. A. M. Abdullah, G. Chen, and J. Chambers, "Optimal downlink transmission for cell-free SWIPT massive MIMO systems with active eavesdropping," *IEEE Trans. Inf. Forensics Secur.*, vol. 15, pp. 1983–1998, 2020.

[36] X. Zhang, W. Cheng, and H. Zhang, "Heterogeneous statistical QoS provisioning over 5G mobile wireless networks," *IEEE Netw. Mag.*, vol. 28, no. 6, pp. 46–53, Nov. 2014.

[37] C.-S. Chang, "Stability, queue length, and delay of deterministic and stochastic queueing networks," *IEEE Trans. Autom. Control*, vol. 39, no. 5, pp. 913–931, May 1994.

[38] X. Zhou, R. Zhang, and C. K. Ho, "Wireless information and power transfer: Architecture design and rate-energy tradeoff," *IEEE Trans. Commun.*, vol. 61, no. 11, pp. 4754–4767, Nov. 2013.

[39] D. S. Michalopoulos, H. A. Suraweera, and R. Schober, "Relay selection for simultaneous information transmission and wireless energy transfer: A tradeoff perspective," *IEEE J. Sel. Areas Commun.*, vol. 33, no. 8, pp. 1578–1594, Aug. 2015.
[40] P. Grover and A. Sahai, "Shannon meets tesla: Wireless information and power transfer," in *Proc. IEEE Int. Symp. Inf. Theory*, 2010, pp. 2363–2367.
[41] B. Clerckx, R. Zhang, R. Schober, D. W. K. Ng, D. I. Kim, and H. V. Poor, "Fundamentals of wireless information and power transfer: From RF energy harvester models to signal and system designs," *IEEE J. Sel. Areas Commun.*, vol. 37, no. 1, pp. 4–33, Jan. 2019.

Xi Zhang (Fellow, IEEE) received the B.S. and M.S. degrees from Xidian University, Xi'an, China, the M.S. degree from Lehigh University, Bethlehem, PA, USA, all in electrical engineering and computer science, and the Ph.D. degree in electrical engineering and computer science (Electrical Engineering-Systems) from The University of Michigan, Ann Arbor, MI, USA.

He is currently a Full Professor and the Founding Director of the Networking and Information Systems Laboratory, Department of Electrical and Computer Engineering, Texas A&M University, College Station, TX, USA. He is an IEEE Fellow for contributions to quality of service (QoS) theory in mobile wireless networks. He was with the Networks and Distributed Systems Research Department, AT&T Bell Laboratories, Murray Hill, NJ, USA, and AT&T Laboratories Research, Florham Park, NJ, in 1997. He was a Research Fellow with the School of Electrical Engineering, University of Technology, Sydney, Australia, and the Department of Electrical and Computer Engineering, James Cook University, Australia. He has published more than 400 research articles on wireless networks and communications systems, network protocol design and modeling, statistical communications, random signal processing, information theory, and control theory and systems. He received the U.S. National Science Foundation CAREER Award in 2004 for his research in the areas of mobile wireless and multicast networking and systems. He was also the recipient of six best paper awards at IEEE GLOBECOME 2020, IEEE ICC 2018, IEEE GLOBECOM 2014, IEEE GLOBECOM 2009, IEEE GLOBECOM 2007, and IEEE WCNC 2010. One of his IEEE JOURNAL ON SELECTED AREAS IN COMMUNICATIONS papers has been listed as the IEEE Best Readings Paper (receiving the highest citation rate among all IEEE transactions/journal papers in the area) on Wireless Cognitive Radio Networks and Statistical QoS Provisioning over Mobile Wireless Networking. He is an IEEE Distinguished Lecturer of IEEE Communications Society and IEEE Vehicular Technology Society. He received TEES Select Young Faculty Award for Excellence in Research Performance from the College of Engineering at Texas A&M University, College Station, in 2006, and the Outstanding Faculty Award from Texas A&M University, in 2020.

Dr. Zhang is serving or has served as an Editor for IEEE TRANSACTIONS ON COMMUNICATIONS, IEEE TRANSACTIONS ON WIRELESS COMMUNICATIONS, IEEE TRANSACTIONS ON VEHICULAR TECHNOLOGY, IEEE TRANSACTIONS ON GREEN COMMUNICATIONS AND NETWORKING, and IEEE TRANSACTIONS ON NETWORK SCIENCE AND ENGINEERING. He served twice as a Guest Editor for IEEE JOURNAL ON SELECTED AREAS IN COMMUNICATIONS for Special Issue on "Broadband Wireless Communications for High Speed Vehicles" and Special Issue on "Wireless Video Transmissions," He was an Associate Editor for IEEE COMMUNICATIONS LETTERS. He served twice as the Lead Guest Editor for *IEEE Communications Magazine* for Special Issue on "Advances in Cooperative Wireless Networking" and Special Issue on "Underwater Wireless Communications and Networks: Theory and Applications." He served as a Guest Editor for *IEEE Wireless Communications Magazine* for Special Issue on "Next Generation CDMA vs. OFDMA for 4G Wireless Applications." He served as an Editor for the Wiley's JOURNAL ON WIRELESS COMMUNICATIONS AND MOBILE COMPUTING, JOURNAL OF COMPUTER SYSTEMS, NETWORKING, AND COMMUNICATIONS, and Wiley's JOURNAL ON SECURITY AND COMMUNICATIONS NETWORKS. He served as an Area Editor for the Elsevier's JOURNAL ON COMPUTER COMMUNICATIONS, and among many others. He is serving or has served as the TPC Chair for IEEE GLOBECOM 2011, the TPC Vice-Chair for IEEE INFOCOM 2010, the TPC Area Chair for IEEE INFOCOM 2012, the Panel/Demo/Poster Chair for ACM MobiCom 2011, the General Chair for IEEE WCNC 2013, and the TPC Chair for IEEE INFOCOM 2017–2019 Workshops on "Integrating Edge Computing, Caching, and Offloading in Next Generation Networks," etc.

Jingqing Wang received the B.S. degree in electronics and information engineering from Northwestern Polytechnical University, Xi'an, China. She is currently working toward the Ph.D. degree under the supervision of Professor Xi Zhang in the Networking and Information Systems Laboratory, Department of Electrical and Computer Engineering, Texas A&M University, College Station, TX, USA. Her research interests include big data based 5G and beyond mobile wireless networks technologies, statistical delay and error-rate bounded QoS provisioning, 6G mURLLC, information-theoretic analyses of FBC, and emerging machine learning techniques over 5G and beyond mobile wireless networks. She won the Best Paper Award from the IEEE GLOBECOM in 2020 and 2014, respectively, the Hagler Institute for Advanced Study Heep Graduate Fellowship Award from Texas A&M University in 2018, and Dr. R.K. Pandey and Christa U. Pandey'84 Fellowship, Texas A&M University, 2020–2021.

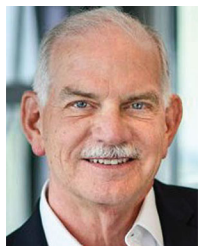

H. Vincent Poor (Life Fellow, IEEE) received the Ph.D. degree in EECS from Princeton University, Princeton, NJ, USA, in 1977. From 1977 until 1990, he was on the faculty of the University of Illinois at Urbana-Champaign, Urbana, IL, USA. Since 1990, he has been on the faculty at Princeton, where he is the Michael Henry Strater University Professor. From 2006 until 2016, he was the Dean of Princeton's School of Engineering and Applied Science. He has also held visiting appointments at several other institutions, including most recently at Berkeley and Cambridge. His research interests include the areas of information theory, machine learning and network science and their applications in wireless networks, energy systems, and related fields. Among his publications in these areas is the forthcoming book *Machine Learning and Wireless Communications* (Cambridge University Press).

Dr. Poor is a Member of the National Academy of Engineering and the National Academy of Sciences, and is a Foreign Member of the Chinese Academy of Sciences, the Royal Society, and other national and international academies. He received the 2017 IEEE Alexander Graham Bell Medal and the 2019 ASEE Benjamin Garver Lamme Award.